

Review

Not peer-reviewed version

Computational Fluid-Structure Interaction in Microfluidics

[Hafiz Muhammad Musharaf](#) , [Uditha Roshan](#) , [Amith Mudugamuwa](#) , [Quang Thang Trinh](#) , [Jun Zhang](#) ^{*} ,
[Nam-Trung Nguyen](#) ^{*}

Posted Date: 1 June 2024

doi: 10.20944/preprints202405.2149.v1

Keywords: Micro elastofluidics; fluid-structure interaction; computational methods; microdevices; cardiovascular modelling



Preprints.org is a free multidiscipline platform providing preprint service that is dedicated to making early versions of research outputs permanently available and citable. Preprints posted at Preprints.org appear in Web of Science, Crossref, Google Scholar, Scilit, Europe PMC.

Copyright: This is an open access article distributed under the Creative Commons Attribution License which permits unrestricted use, distribution, and reproduction in any medium, provided the original work is properly cited.

Review

Computational Fluid-Structure Interaction in Microfluidics

Hafiz Muhammad Musharaf ¹, Uditha Roshan ¹, Amith Mudugamuwa ¹, Quang Thang Trinh ¹, Jun Zhang ^{1,2,*} and Nam-Trung Nguyen ^{1,*}

¹ Queensland Micro and Nanotechnology Centre, Griffith University, Brisbane, QLD 4111, Australia.

² School of Engineering and Built Environment, Griffith University, Brisbane, QLD 4111, Australia.

* Correspondence: jun.zhang@griffith.edu.au (J.Z.); nam-trung.nguyen@griffith.edu.au (N.-T.N.)

Abstract: Micro elastofluidics is a transformative branch of microfluidics, leveraging fluid-structure interaction (FSI) at the microscale to enhance the functionality and efficiency of various microdevices. This review paper elucidates the critical role of advanced computational FSI methods in the field of micro elastofluidics. By focusing on the interplay between fluid mechanics and structural responses, these computational methods facilitate the intricate design and optimisation of microdevices such as microvalves, micropumps, and micromixers, which rely on the precise control of fluidic and structural dynamics. In addition, these computational tools extend to the development of biomedical devices, enabling precise particle manipulation and enhancing therapeutic outcomes in cardiovascular applications. Furthermore, this paper addresses the current challenges in computational FSI and highlights the necessity for further development of tools to tackle complex, time-dependent models under microfluidic environments and varying conditions. Our review highlights the expanding potential of FSI in micro elastofluidics, offering a roadmap for future research and development in this promising area.

Keywords: micro elastofluidics; fluid-structure interaction; computational methods; microdevices; cardiovascular modelling

1. Introduction

Microfluidics, encompassing the manipulation and control of fluids within networks of channels with typical dimensions ranging from 0.1 μm to 100 μm , offers distinct advantages compared to traditional laboratory-scale techniques. The square-cube law implies that as device dimensions decrease, heat and mass transfer in a microfluidic device can be significantly improved. Microfluidic devices also facilitate faster and more efficient separation processes. Their high surface-to-volume ratio facilitates rapid modifications in fluid dynamics essential for effective separation. Additionally, precise fluid control and integrated functionalities within these devices allow for enhanced reaction kinetics and reduced process steps, making them ideal for applications in biochemical assays, environmental monitoring, and medical diagnostics [1–4].

Micro elastofluidics is an emerging and promising research field of microfluidics. Micro elastofluidics was first introduced by Nguyen [5] and holds considerable potential for a variety of applications including particle/cell separation [6–8], controlled drug release [9], tuneable optofluidic devices [10], tuneable droplet-size generation [11], capillary flow enhancement [12], mixing [13,14], and the development of fluidic circuits [15,16].

Despite recent advancements in flexible microfluidic devices, such as those designed for wearable applications, phenomena arising from fluid-structure interaction at both molecular and device scales have yet to be fully explored. The field of micro elastofluidics will benefit from substantial advancements in computational Fluid-Structure Interaction (FSI) methods [17–19]. These computational techniques are crucial for designing, optimizing, and understanding mechanisms that

rely on the intricate interactions between fluidic and structural dynamics at the microscale. In micro elastofluidics, these models could also predict the deformation of microstructures and microchannels due to fluid flow and vice versa. In this context, the incorporation of reliable FSI models is crucial for accurately forecasting interconnected physical phenomena. Utilizing high-fidelity simulations enables a thorough examination of the specific application, taking into account all relevant scales involved.

This review paper highlights the instrumental role of computational methods such as Finite Element Method (FEM), Boundary Element Method (BEM), Molecular Dynamics (MD), Lattice Boltzmann Method (LBM), and Immersed Boundary Method (IBM) in advancing FSI for micro elastofluidics. Each of these methods offers distinct advantages and faces specific challenges, making their study and application crucial for the development of microfluidic devices. We also explore the application of computational FSI methods, highlighting their impact on the development of microdevices such as microvalves, micropumps, and micromixers, **Figure 1**. These devices utilise the principles of FSI to enhance their performance and functionality, adapting to the dynamic nature of interactions between fluid flow and elastic structures. Microvalves, for example, benefit from FSI models for optimised flow control, ensuring that they can operate under varying pressures and fluid properties. Micropumps are devices, where FSI is indispensable for optimising pump efficiency and reliability under diverse operation conditions.

Moreover, designing micromixers utilises FSI to refine the geometries and mixing mechanisms, enabling effective mixing of fluids at low Reynolds numbers which are typical in microfluidics. The precise control and enhanced mixing derived from FSI models are vital for applications ranging from chemical synthesis to biological assays.

Beyond device-specific applications, computational FSI methods play a transformative role in biomedical applications such as cell separation and particle manipulation. These processes require not only precision but also gentle handling of delicate biological specimens, which can be achieved through well controlled microenvironment, as facilitated by FSI modelling. In addition, cardiovascular applications of FSI in micro elastofluidics have gained recent attention. FSI models are essential for designing cardiovascular devices that mimic or interact with biomechanical properties of tissues, improving therapeutic outcomes and patient-specific treatments. This review also discusses the challenges and future directions in the computational aspect of FSI in micro elastofluidics, including the need for more sophisticated models that can accurately predict complex interactions in real-time and under variable operation conditions. The continued evolution of computational tools and techniques is likely to further enhance the capabilities and applications of FSI in micro elastofluidics, marking an exciting frontier for both fundamental research and practical applications.

Overall, the integration of computational FSI methods into micro elastofluidics represents a significant stride towards more advanced, efficient, and versatile microfluidic systems. Through detailed case studies and theoretical analyses, this review aims to provide a comprehensive overview of the current state and promising future of FSI in this innovative field, encouraging further research and development.

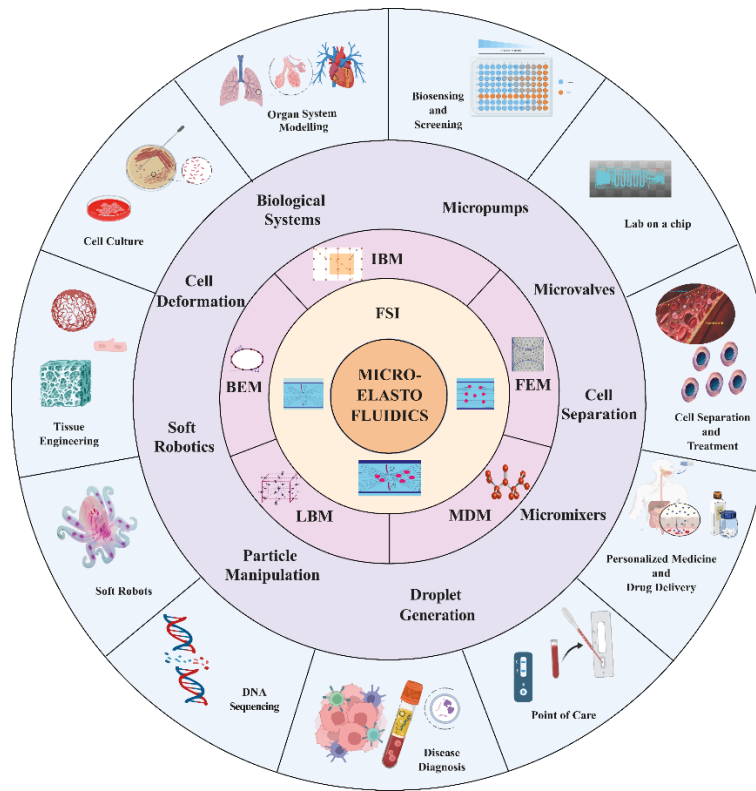


Figure 1. A schematic overview of applications of computational methods in FSI for micro elastofluidics.

2. Fundamentals of Fluid-Structure Interaction in Micro Elastofluidics

In microfluidics, channels, and structures with dimensions on the order of micrometres are commonly used to manipulate and control fluid behaviour [20]. Microchannels have been utilised to solve small-scale flow and fluid manipulation tasks within microfluidic devices. Polydimethylsiloxane (PDMS) is a popular material for making microchannels owing to its cost-effectiveness, ease of use, transparency, biocompatibility, and elasticity [4,21–24]. The low Young modulus of PDMS allows for emulating blood vessels and soft organs in biomedical studies [25]. Nevertheless, its elasticity poses challenges in both experimental and theoretical modelling due to its susceptibility to change of channel geometry induced by the flow, and in turn, affecting the overall hydrodynamic behaviour of the device.

In many microfluidic applications, the wall of microchannels is flexible or stretchable to adapt to biological systems, leading to the introduction of the new subfield micro elastofluidics [5]. Micro elastofluidics is further categorised as digital and continuous-flow micro elastofluidics. Digital micro elastofluidics is based on elastic capsules or deformable beads flowing in the fluid. Continuous micro elastofluidics is based on deformable structures and their interactions with the fluid. Both branches have their unique features and applications. For example, elastic capsules [26] can be used for drug delivery and liquid storage, while stretchable pump [27] is the perfect example of continuous-flow micro elastofluidics.

In micro elastofluidics, unique features of microfluidics such as flow regime, surface tension, diffusion, fluidic resistance, and inertial and shear forces play the same roles in flow behaviour. Fluid flow is usually laminar in micro elastofluidics since the Reynolds Number ($Re = \frac{\rho v D_h}{\mu}$) in most applications is less than 1. Although high flow regimes may have Re in the range of 10–100. Surface tension, arising from cohesive forces between liquid molecules, is relatively strong within a microfluidic system and can be determined through the Young-Laplace equation ($\Delta P = \gamma(\frac{1}{R_1} + \frac{1}{R_2})$) [28,29], where ΔP represents the pressure difference, γ is the surface free energy of the liquid, and R_1 and R_2 denotes the radii of curvature, perpendicular and parallel to the liquid flow, respectively

Diffusion, the spreading of particles due to random Brownian motion, is determined by Einstein-Smoluchowski theory ($d^2 = 6Dt$), where d is the distance travelled by the particle, t is time and D is the coefficient of diffusion. Fluidic resistance (R) analogous to electrical resistance, dictates how easily fluids move through microchannels ($Q = \frac{\Delta P}{R}$), where Q is the flow rate and ΔP is the pressure drop across the channel. The fluidic resistance can be calculated using formulas specific to channel shape [30,31]. Due to the flexible and stretchable nature of the channels or particles, an added physics of fluid-structure interaction is necessary to comprehend the fluidic phenomena in the device. In the next section, we will discuss how structural deformability interacts with the flow of fluid and vice versa.

2.1. Fundamentals of Fluid-Structure Interaction

In micro elastofluidics, the study of FSI is crucial for understanding the behaviour of fluids confined in flexible microchannels and the impact of this behaviour on the surrounding structures. As described by Duprat and Stone [32], FSI denotes mechanical problems where the flow field affects the orientation, shape, and location of an interacting object, leading to reciprocal modifications in the flow pattern. The flexible and elastic nature of the microchannel does not allow the use of already established rules of rigid microfluidics and necessitates the incorporation of fluid-structure interaction to obtain suitable engineering solutions.

The focus of FSI is on the coupling between fluid dynamics and structural mechanics. Fluid flow exerts forces on a structure, potentially causing it to deform. The magnitude of these deformations depends on fluid pressure, velocity, and material properties of the structure. Minor deformations may not significantly affect the fluid flow. However larger deformations create a feedback loop where the altered structure modifies the behaviour of the fluid. FSI with negligible influence of deformation on fluid flow is considered as one-way fluid-structure interaction. Problems with one-way FSI are relatively easy to manage and comprehend. Two-way or fully coupled FSI induces deformation large enough to affect the fluid flow, which in turn significantly changes the flow-induced deformation of the structure, **Figure 2**. These complex interactions are important for biomedical problems such as blood flow in flexible vessels [33], and designing medical devices such as micropumps [27,34].

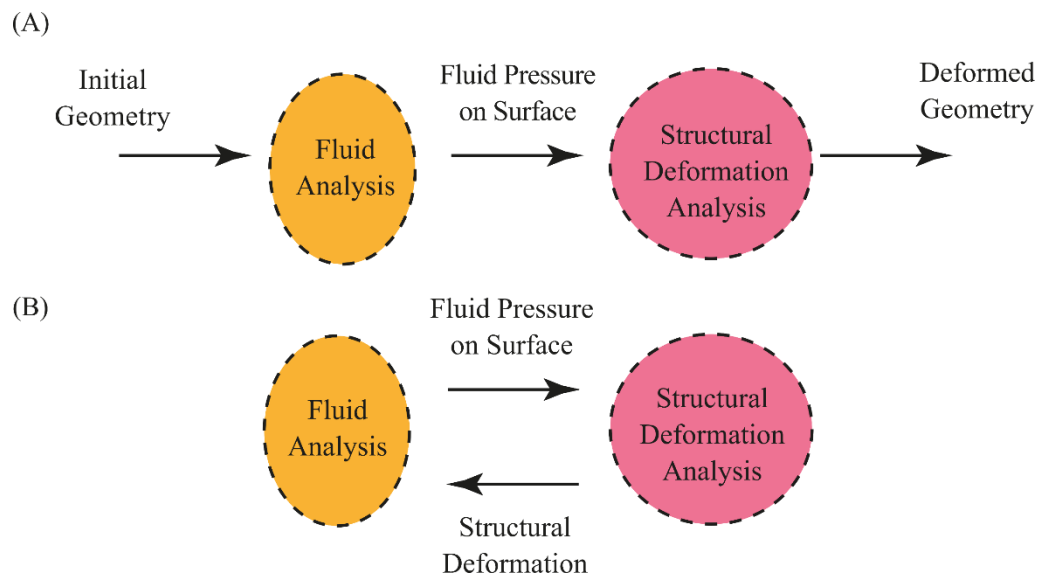


Figure 2. Fluid structure interaction: (A) One-way FSI, (B) Two-way FSI.

Considering the interface between fluid and a deformable structure, FSI can also be categorised further into two types (i) fluid-wall interface and (ii) fluid-particle interface, **Figure 3**. In FSI with the fluid-wall interface, deformable structures are walls of microchannels, **Figure 3A**. These walls are elastic, flexible, and fixed. For example, in continuous micro elastofluidics, walls of microchannel can be bent and stretched but cannot move. Hence, analysing continuous micro elastofluidic problems

should consider FSI with fluid-wall interface. In FSI with the fluid-particle interface, deformable structures are moving particles, **Figure 3B**. These particles are elastic and deformable but are not fixed at a point. Fluid forces cause the cell to deform as well as change its position, and these changes in shape and position alter the pattern of fluid flow. For instance, problems related to digital micro elastofluidics are analysed through FSI with the fluid-particle interface. Methods have been developed to study this FSI at the particle boundary, with applications in cell sorting and biomechanics of cells.

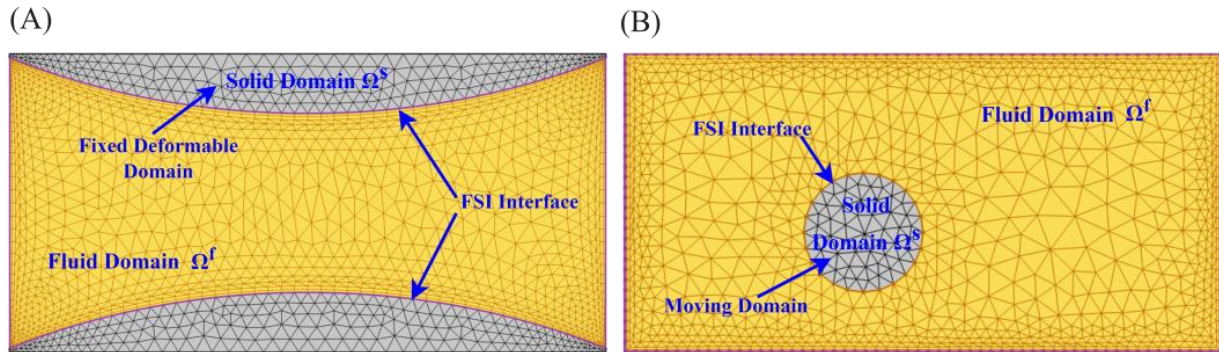


Figure 3. (A) Fluid-wall FSI, (B) Fluid particle FSI.

Understanding the relationship between volumetric flow rate Q and pressure drop ΔP is crucial for the design and operation of fluidic systems. In deformable microchannels, this $\Delta P - Q$ relationship is nonlinear, which is a major difference to flow in rigid microchannels [35]. Deformation of channel walls reduces flow resistance, causing lower pressure drop [19,36]. To elucidate this relationship, numerous experimental works have been conducted, and researchers have developed empirical models for pressure-flow characteristics. For instance, Gervais *et al.* [35] investigated the behaviour of fluid flow in stretchable microchannels using confocal microscopy. A model was created to describe the observed pressure-flow characteristics. The results indicate that flexible microchannels could enable higher flow rates compared to rigid microchannels of identical size driven by the same pressure difference. Subsequently, Hardy *et al.* [37] investigated the behaviour of PDMS microchannels with flexible walls and reported significant differences in pressure drop compared to rigid channels. The team demonstrated that pressure drop in flexible microchannels decreases down to 35% of that in identical channels with rigid walls.

Another FSI problem is compressible flow in deformable channels. The mass flow rate is a function of, undeformed microchannel dimensions, differential pressure across a microchannel, and characteristics of the channel's surface such as elastic modulus, thickness, and Poisson's ratio [19,36,38–44]. Although efforts have been made toward the development of empirical models for the $\Delta P - Q$ relationship, these models only apply to specific conditions with small domain characteristics. To comprehend the generalised and complete FSI phenomena, numerical analysis is necessary. The next section discusses fluid dynamics and solid mechanics of FSI and its governing equations.

2.2. Fluid Dynamics and Solid Mechanics of FSI

Understanding the fluid dynamics of FSI poses a multifaceted challenge for the design and applications of micro elastofluidic devices. Key considerations include the dominant role of surface tension, potential hyperelastic responses of the elastomeric materials, and the two-way dynamic coupling between fluid stresses and structural deformations. Analytical solutions are rarely feasible for FSI problems, and lab experiments can't capture the full range of behaviours. These bottlenecks make numerical simulations crucial for understanding the complex physics of how fluids and solids interact. Understanding FSI in microfluidics has been advanced through the development of dimensionless continuum finite approaches (FEM, BEM) and digital finite approaches (MDM and LBM) [45]. These methods are discussed thoroughly in the next section.

FSI involves the fluid dynamics as well as solid mechanics of stretchable solids containing the fluid or surrounded by the fluid. Without the effect of flexible structure on the flowing fluid, the behaviour of fluid is governed by the equation of continuity:

$$\nabla \cdot \mathbf{u} = 0 \quad (1)$$

and Navier-Stokes equation:

$$\rho \left(\frac{\partial \mathbf{u}}{\partial t} + (\nabla \cdot \mathbf{u}) \mathbf{u} \right) = -\nabla p + \mu \nabla^2 \mathbf{u} + \mathbf{F} \quad (2)$$

where ρ , \mathbf{u} , p , μ are the fluid density, vector velocity, pressure, and dynamic viscosity respectively, t is the time and \mathbf{F} represents the external body force.

The body force \mathbf{F} in FSI is introduced by the flexible structure. This force can be applied externally on the deformable structure to simplify the problem in one-way FSI. Alternatively, this force can be induced in the structure by the flowing fluid in coupled FSI hence making the problem more precise in expense of complexity. This induced force depends on the nature of the material and the behaviour of the flexible structure under stress and strain.

In the solid domain, the equations of motion are typically described by the linear elasticity equations, assuming small deformations. The governing equation is the linearised form of the momentum balance equation [46]:

$$\rho_s \frac{\delta^2 \mathbf{d}_s}{\delta t^2} = \nabla \cdot \boldsymbol{\sigma} \quad (3)$$

where, ρ_s is the density of the solid, \mathbf{d}_s represents the displacement vector of the solid and $\boldsymbol{\sigma}$ is the stress tensor.

The constitutive relation between stress and strain (Hooke's law) is often utilised, linking stress $\boldsymbol{\sigma}$ to strain $\boldsymbol{\epsilon}$ via Lame's equation of deformation [47]:

$$\boldsymbol{\sigma} = \lambda t_r(\boldsymbol{\epsilon}) \mathbf{I} + 2\mu \boldsymbol{\epsilon} \quad (4)$$

where $\lambda = \frac{E\nu}{(1+\nu)(1-2\nu)}$ is Lamé's first parameter, representing the material's compressibility since ν is the Poisson's ratio of the material, $t_r(\boldsymbol{\epsilon})$ is the trace of the strain tensor $\boldsymbol{\epsilon}$, which corresponds to the volumetric strain, $\mu = \frac{E}{2(1+\nu)}$ is Lamé's second parameter, also known as the shear modulus, characterizing the material's resistance to deformation and \mathbf{I} is the identity tensor. The term $\lambda t_r(\boldsymbol{\epsilon}) \mathbf{I}$ accounts for the isotropic (volumetric) deformation. This term is then multiplied by the identity tensor \mathbf{I} , indicating that this part contributes to the isotropic stress or hydrostatic pressure component. The term $2\mu \boldsymbol{\epsilon}$ represents the deviatoric deformation, accounting for the deformation that leads to shape changes without altering the volume.

The overall equation combines these two components to describe the complete stress tensor $\boldsymbol{\sigma}$ in the context of fluid-structure interaction. It reflects the material response to both isotropic and deviatoric deformations induced by external forces or fluid interactions. Modelling FSI in micro elastofluidic devices, where fluid flow deforms elastomeric structures, requires specialised approaches. Hyperelastic material models, capable of handling large deformations, are to be considered for accurate results. Many constitutive models have been formulated to characterise the nonlinear mechanical behaviour of hyperelastic materials. Within this theoretical framework, the Neo-Hookean [48] and Mooney-Rivlin [48] models stand out as widely adopted approaches for describing large deformations, which are characteristic of elastomers.

2.3. Boundary Conditions

In FSI problems, boundary conditions define the constraints and interactions that shape the behaviour of the system. Three distinct types of boundaries are considered for micro elastofluidic applications: (i) boundary conditions at the device surface that may be moving in stretchable microfluidics; (ii) boundary conditions related to the surface of particles that also may be in motion and potentially changing shape; (iii) inlet and outlet conditions, due to open-system nature of microfluidic devices, **Figure 4**.

In most cases, device surfaces are considered impermeable and under the no-slip condition. These surfaces are typically regarded as rigid and stationary. Thus, the interaction between the device and the flowing fluid is primarily defined by the static nature of the channel wall and the no-slip condition. However, device walls are deformable in flexible microchannels. Thus, boundary

conditions at the device surfaces change with time. We can incorporate these changes in FSI simulations as a moving boundary condition.

The study of elastic particle transport requires modelling of FSI at particle boundaries. These interactions encompass both velocity and stress continuity. The movement and alteration of particles impact the flow and are reciprocally influenced by it, thereby establishing an FSI problem. Hydrodynamic forces and torque on particles determine the translation, rotation, and deformation of the particle surface. These phenomena on particles are studied under Inertial Particle Microfluidics (IPMF). Force and torque acting on particles are calculated as:

$$F = \oint dA \sigma \cdot n \quad (5)$$

$$T = \oint dA x \times (\sigma \cdot n) \quad (6)$$

In these equations, σ , n , and x represent the fluid stress tensor, unit vector normal to the surface, and the spatial position of a point on the surface of the particle respectively.

Probably, the most difficult part of IPMF is numerically solving the FSI problem. Additional forces may become noticeable as particles move close to each other or close to the device's surface. These forces either have chemical (electrostatic interactions, adsorption phenomena, surface chemistry effects, and chemical gradients) or physical origins (inertial and viscous drag forces, along with lift and Dean forces). Physical factors such as gravitational and buoyancy forces become insignificant in IPMF because of high fluid stress and low volume [49]. For considering the elastic behaviour of particles in IPMF, a suitable elastic constitutive model must be selected to describe the particle's deformation under hydrodynamic stresses.

The inlet and outlet conditions hold significant importance for modelling fluid-structure interaction in micro elastofluidics. In reality, where only specific parts of a device are pertinent or feasible for simulations, it is crucial to define the flow at the planes of the inlet and outlet of the selected variable. For subsets representing straight channels or unit cells with periodic characteristics such as serpentine channels, periodic boundary conditions usually provide the best and most direct solution. Any particle or liquid leaving one side of the numerical domain enters again into the other side. Essentially, the model is an unlimited collection of unit cells, with the stimulated domain serving as the definition of each unit cell.

On the other hand, periodic boundary conditions are not suitable for subsets with intricate shapes. In such cases, pressure and volume conditions are important at the inlet and outlet. For an unknown flow field at the inlet plane, modelers use a velocity profile to characterise flow within a specified channel geometry, which presumes no upstream perturbations. For a variety of geometrically simple cross-sections, time-independent closed-form solutions of Navier-Stokes equations for duct pipes are available [50], making them an obvious choice for creating a comprehensive velocity profile.

Since flow within the stimulated domains determines the outlet plane flow field, and flow perturbations upstream outside of the domain are minimal, it becomes easier to control the outlet. An alternative outflow condition, often used instead of periodicity, is a zero-gradient condition [51]. Additionally, non-periodic boundary conditions introduce complexities in handling particles entering and exiting the subset.

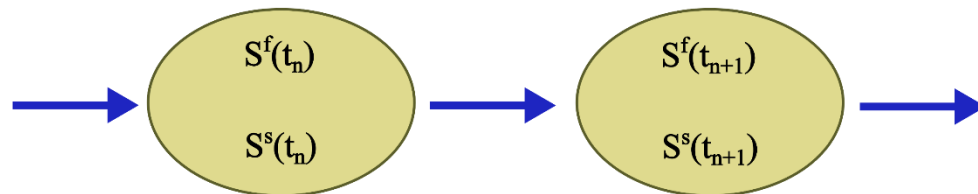
2.4. Coupling Approaches

The selection of a suitable coupling approach is the cornerstone of successful FSI simulation. This determines the mechanism by which the fluid and structure domains exchange displacement and force information at the interface during iterative solutions or time steps. The selected coupling strategy can significantly impact the numerical stability, convergence rate, and the ability to capture the true physics of the coupled system.

Two primary approaches exist: monolithic and partitioned, **Figure 5**. In monolithic approaches, the governing equations for fluid and solid domains are integrated into a single, unified framework and solved simultaneously. Interfacial boundary conditions (e.g., no-slip, stress continuity) are implicitly embedded within this framework. Monolithic schemes offer superior accuracy for tightly coupled FSI problems but often demand the development of highly specialised solvers, potentially

increasing implementation complexity and computational expense [52–54]. In contrast, the partitioned approach considers the fluid and structure as separate computational domains. This approach enables the independent discretization of each domain and the application of numerical solution techniques optimised for the governing physics within each domain. The approach allows for the use of specialised, potentially pre-existing "legacy" solvers optimised for each respective physical domain (e.g., fluid vs. structural mechanics). Interfacial data exchange (displacements, tractions) occurs iteratively, potentially simplifying development time and enhancing flexibility. However, careful attention must be paid to interface tracking and the stable, accurate transfer of data across this dynamic interface. Specialised algorithms designed for moving boundary problems are often required to ensure numerical stability and prevent unphysical solution behaviour.

(A) Monolithic Approach



(B) Partitioned Approach

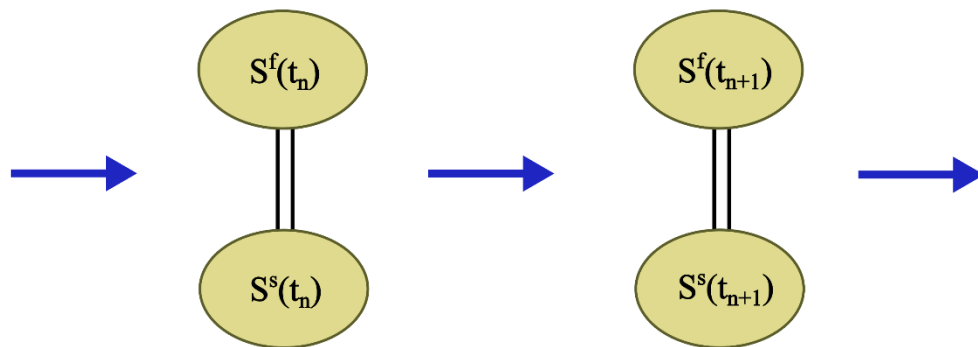


Figure 5. FSI coupling approaches, (A) Monolithic, (B) Partitioned.

An additional classification scheme for the FSI solution is based on the discretization of mesh, which dictates how interfacial boundary conditions are imposed within the discretised system of equations, **Figure 6**. One is the Conforming Meshing Method, where the fluid-structure interface is considered as a physical boundary. The fluid and solid domain meshes must perfectly match. This often leads to re-meshing (or mesh-updating) as the structure deforms throughout the simulation, hence adding computational cost. The other is the Non-Conforming Meshing Method, where the fluid-structure interface is not treated as a strict alignment boundary. Instead, the interface location and its conditions (e.g., stress continuity) are considered constraints within the governing equations. This approach enables independent meshing for each domain, streamlining simulation setup and avoiding re-meshing.

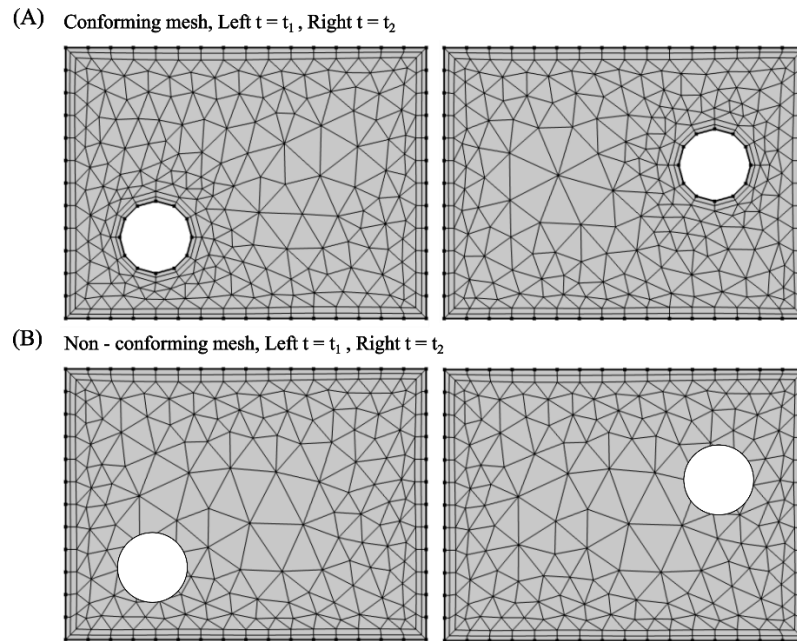


Figure 6. Mesh discretization approaches, (A) Conforming meshing, (B) Non-conforming meshing.

3. Computational Methods for Studying Fluid-Structure Interactions

Numerical simulation techniques play a crucial role in science and engineering, enabling researchers to study complex phenomena and make predictions based on mathematical models. In recent years, computational methods have played a significant role in studying FSI, providing valuable insights into the behaviour of fluids and structures. In the field of micro elastofluidics, numerical methods have been used in the design, analysis, and optimization of micro elastofluidic devices. Additionally, numerical approaches such as FEM, BEM, MD, and LBM allow for discretisation and solving the governing equations of fluid dynamics and hyperelasticity with their intricate coupling at the fluid-structure interface. These methods are indispensable for predicting flow patterns, understanding how microstructures deform under fluid stresses, and designing novel micro elastofluidic devices. Notably, these numerical approaches enable the exploration of a wide parameter space far beyond what may be accessible experimentally, aiding the optimization and development of devices for applications ranging from biomedical diagnostics to soft micro-robotics. Furthermore, the application of these numerical methods extends to various fields, including the development of passive microvalves [55,56], and micromixers [57–59], to understand the fluid dynamics and to optimise the performance of these devices. Extensive numerical methods have been developed and refined for microfluidic applications such as biosensors [60,61], and biofluid handling [62] in wearable devices. However, the emerging field of micro elastofluidics warrants further advancements due to the inherent complexities of fluid-structure interactions in the microscale. Therefore, numerical methods are integral to gaining insights into the complex fluid-structure interactions and optimizing the performance of micro elastofluidic systems. This section discusses comprehensively all numerical methods that can be used for FSI in micro elastofluidics. **Figure 7** illustrates the different computational methods in space and time scale.

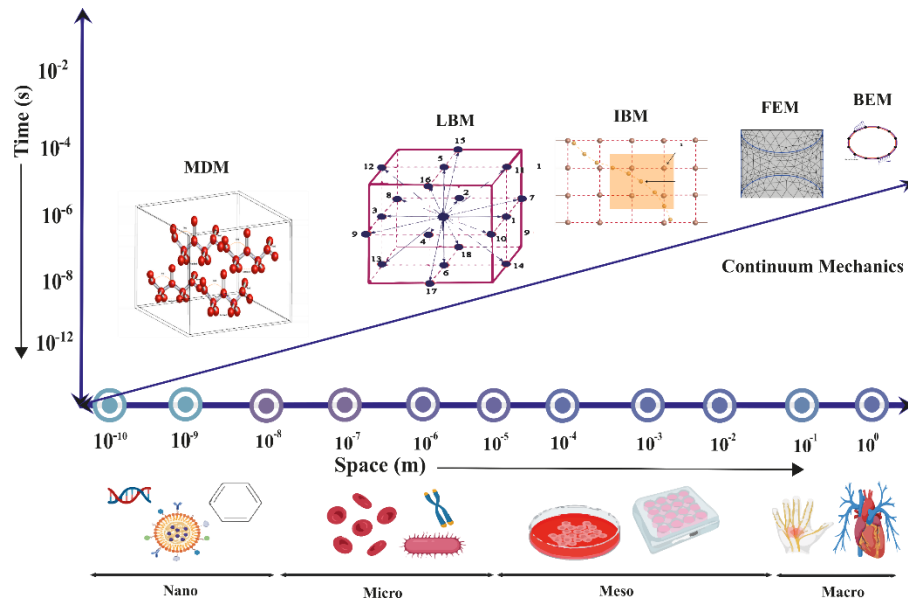


Figure 7. Space and Time scale of different computational methods application.

3.1. Finite Element Method

The Finite Element Method (FEM) is an indispensable computational tool for tackling the complex challenges presented by FSI in micro elastofluidics. This method divides the domain of interest into smaller elements, allowing for the accurate modelling of complex geometries and boundary conditions, **Figure 8A**. FEM has been widely applied in various aspects of microfluidics. Hung *et al.* [63] modelled mass transfer using FEM in a high-aspect ratio microfluidic device, which provides a stable and uniform microenvironment for cell growth in a high-throughput mammalian cell culture array. Erickson *et al.* [64] investigated the role of surface heterogeneity on electrokinetically driven microfluidic with 3D FEM, aiming to enhance mixing in a T-shaped micromixer. Bianchi *et al.* [65] implemented FEM models to simulate electroosmotic-driven flow division at a T-junction.

FEM has also been applied in various contexts to investigate fluid-structure interactions in microfluidics. For example, Zhang *et al.* [66] reported a groundbreaking application of the Cell-based Smoothed Finite Element Method (CS-FEM) to computational fluid dynamics (CFD) and FSI simulations. CS-FEM belongs to the broader family of Smoothed Finite Element Methods (S-FEM), which aim to enhance accuracy and robustness by applying strain smoothing techniques. Specifically, CS-FEM simplifies calculations by not requiring explicit shape functions and demonstrates better tolerance to distorted meshes. This study demonstrated that CS-FEM offers greater accuracy and stability in handling deformable interfaces and flow fields that typify FSI problems, making it well-suited for simulations relevant to micro elastofluidics. Erickson *et al.* [67] applied the same approach to investigate how smart one-way micro-valves behave when FSI is taken into account. Hence, FEM has been proven vital in comprehending FSI in micro elastofluidics.

A typical FEM approach consists of five steps: (i) Discretization: The continuum domain is discretised into a finite number of smaller elements that are easier to manage; (ii) Element Equation Formulation: For each element, the governing physical equations are formulated. These equations typically stem from fundamental conservation laws (such as mass, momentum, and energy conservation) and are expressed in terms of local element variables; (iii) Assembly: The local element equations are assembled into a global system of equations that models the entire problem domain. This step involves integrating the contributions of individual elements to the overall behaviour of the system; (iv) Solution: The global system of equations is solved numerically to find the unknowns, such as displacements and pressures. This solution process may incorporate iterative methods and solvers that handle non-linearities and complex boundary conditions; (v) Post-processing: The solution obtained is interpreted in terms of physical quantities of interest, such as stress distributions,

fluid velocities, and pressures. This helps in evaluating the performance and safety of the micro elastofluidic devices. FEM for simulating FSI in micro elastofluidics consists of modelling the fluid domain, modelling the deformable structure domain, and then fluid-structure interface coupling. In every phase, specific mesh strategy and physics are used to simulate and then coupled them. Here we discuss physics and governing equations of these domains.

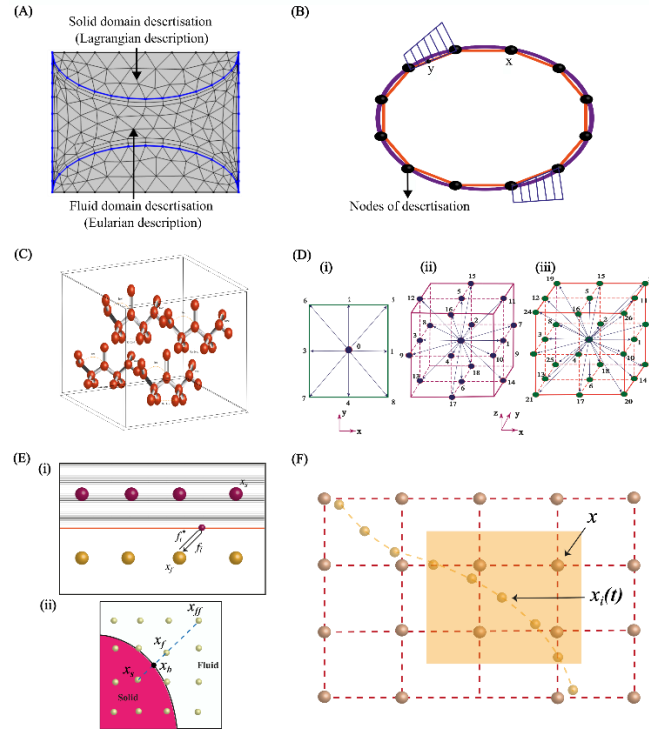


Figure 8. Computational methods for FSI. (A) Discretisation of fluid and solid domain in FEM; (B) Discretisation of domain in BEM; (C) Molecules interaction in MD method; (D) 2D and 3D configurations of LBM; (E) (i) Bounce Back Method, (ii) Extrapolated Bounce Back Method illustration; (F) IBM as Lagrangian and Eulerian description.

3.1.1. Modelling of Fluid Domain

FEM begins by discretizing the fluid domain (e.g., a microfluidic channel) into a mesh of smaller, interconnected elements. These elements are often triangles or quadrilaterals in 2D and tetrahedra or hexahedra in 3D. In this domain, FEM describes the mesh as Eulerian space. The behaviour of the fluid within this mesh is governed by the fundamental Navier-Stokes equations. These equations express the conservation of mass i.e. **equation (1)** and momentum i.e. **equation (2)**. To solve the Navier-Stokes equations numerically, FEM employs a technique called the Galerkin method. Essentially, the equations are transformed into their 'weak form' and approximated using shape functions. These shape functions describe how the fluid velocity and pressure vary within each element of the mesh. The introduction of shape function in simulations is defined as:

$$u(x) = \sum N_i(x)u_i \quad (7)$$

$$p(x) = \sum M_j p_j \quad (8)$$

where; $N_i(x)$ is the shape function and u_i is the nodal velocity. Similarly, in **equation (8)**, M_j is the shape function and p_j is the nodal pressure.

3.1.2. Modelling of Deformable Structure

The versatility of FEM extends to handling solid mechanics of deformable structures interacting with the flow. FEM divides the structural domain in the same way as the fluid domain, i. e. into small finite elements. However, the structural domain uses Lagrangian description. The governing equations of solid mechanics i.e. **equation (9)** describe the balance of forces within the structure and

the relationship between stress and strain (deformation). The choice of a constitutive model (e.g., linear elastic, hyperelastic, viscoelastic) dictates how the material responds to these stresses. Similar to the fluid domain, FEM discretises deformable structures with elements and uses shape functions to approximate the displacement field.

$$\nabla \cdot \sigma + f_s = 0 \quad (9)$$

$$d(x) = \sum X_i d_i \quad (10)$$

where σ is the stress tensor and f_s is body force on the structure. More importantly, this body force comes from fluid pressure on the structure in FSI problems. In **equation (10)**, $d(x)$ is the displacement vector and X_i is the shape function and d_i is the nodal displacement vector. For micro elastofluidics, selecting the appropriate shape functions is crucial and directly depends on the material models used to represent the deformable structures. For materials exhibiting linear elastic behaviour, where deformations are small, linear or quadratic shape functions often provide sufficient accuracy. However, microfluidic systems often involve significant deformations, demanding the use of hyperelastic material models. These models describe nonlinear stress-strain relationships, thus necessitating higher-order shape functions within FEM to accurately represent the complex deformation patterns that can occur.

3.2. Boundary Element Method

The Boundary Element Method (BEM) is another numerical technique for solving problems involving FSI in microfluidics. Analysing the behaviour of fluids and structures at the boundaries of microfluidic devices is one of the advantage of BEM. Unlike FEM, which divides the entire domain into smaller elements, BEM is based on discretizing the boundary of the domain of interest as shown in **Figure 8B**.

For FSI in micro elastofluidics, BEM converts the governing partial differential equations (PDEs) of fluid dynamics and structural mechanics into boundary integral equations using appropriate Green's functions [68]. The integral equations for both the fluid and structural domains are discretised using boundary elements. The interactions are numerically integrated across each element. This step involves the computation of governing coefficients, which quantify the effect of one element on another across the fluid-structure interface. The discretised equations form a system of linear algebraic equations, which are solved to ascertain the unknown boundary values, such as fluid pressures and structural displacements. This resolution often employs iterative methods, especially when the interaction between fluid and structure exhibits significant nonlinearity. After computing the boundary values, further calculations are conducted to evaluate other internal fields as required. For micro elastofluidic devices, this may involve determining fluid velocity field or stress distribution within the structural material, vital for the thorough analysis and design of the devices.

The formulation of integral equations in BEM is crucial for solving problems involving FSI in micro elastofluidics. Integral equations are derived from the domain's governing differential equations using mathematical techniques involving Green's functions. Green's functions are specific solutions to differential equations under impulse (or point source) conditions and are fundamental to problems in physics and engineering. Essentially, these functions describe how effects (such as stress, heat, or electromagnetic fields) propagate from a source point to an observation points in space.

BEM uses Green's functions to convert the local description of the phenomena (differential equations) into a global one (integral equations) over the boundary. This conversion is based on boundary integral theorems such as Green's theorem in potential theory or Kelvin's theorem in elasticity [69], which relates the values of a function inside a domain to values on the domain's boundary. The specific Green's function depends on the type of differential equation and the nature of the domain (e.g., infinite space, half-space, bounded domain). Once the appropriate Green's function is selected, the integration over the boundary can be set up. This step is crucial because it reduces the problem from a volumetric one to a surface-based one, significantly simplifying the computational domain and potentially reducing the amount of computational effort required. However, accurately computing Green's functions and their integrals over complex boundary shapes

can be mathematically and numerically challenging, often requiring sophisticated numerical integration techniques and careful handling of singularities.

For fluids, particularly under the assumption of potential flow, which is common in many microfluidic applications due to the low Reynolds number, the fluid behaviour can be described by the Laplace equation for the potential ϕ , where $\nabla^2 \phi = 0$. The integral equation for the fluid potential, derived from the Laplace equation is expressed as [68]:

$$\phi(x) = \int_{\Gamma} \phi(y) \frac{\partial G(x,y)}{\partial n_y} dS_y - \int_{\Gamma} G(x,y) \frac{\partial \phi(y)}{\partial n_y} dS_y \quad (11)$$

where $\phi(x)$ is the potential at the point (x) , $G(x,y)$ is Green's function for the Laplacian, applicable to the boundary conditions and geometry of the fluid domain, Γ denotes the boundary of the domain, $\frac{\partial}{\partial n_y}$ represents the derivative normal to the boundary at point y , dS_y is the differential boundary element at y . This equation effectively transforms the volumetric problem of fluid dynamics into a surface problem, simplifying the computational domain to just the boundaries where fluid and structural interactions occur.

For the structural component, when considering elastic behaviour under small deformations, the displacement field \mathbf{u} in the structure can be described using linear elasticity. Assuming isotropic and homogeneous material properties, the corresponding integral equation derived from the Navier-Cauchy equations for elasticity is [68]:

$$\mathbf{u}(x) = \int_{\Gamma} \mathbf{T}(y,x) \mathbf{u}(y) dS_y - \int_{\Gamma} \mathbf{U}(y,x) \mathbf{t}(y) dS_y \quad (12)$$

where $\mathbf{u}(x)$ is the displacement at point x , $\mathbf{T}(y,x)$ and $\mathbf{U}(y,x)$ are the traction and displacement kernels derived from the fundamental solutions of elasticity, $\mathbf{t}(y)$ represents the traction at point y on the boundary Γ .

Coupling at the fluid-structure interface requires that the fluid forces e.g., pressure and shear stress derived from the fluid potential ϕ and the structural responses such as displacements and stresses, accurately match at the interface. Kinematic continuity ensures that the displacement of the structure matches the fluid displacement at the boundary. Dynamic continuity ensures that the sum of stress vectors from both fluid and structure at their interface is zero, maintaining force balance. This is achieved by ensuring the continuity of displacements and tractions across the interface, linking the fluid and structural integral equations. These coupled equations are then solved iteratively or simultaneously to yield the interaction dynamics essential for device functionality. This coupled approach, facilitated by BEM, allows for a sophisticated analysis of interactions in micro elastofluidic devices, providing critical insights into device performance and guiding design optimizations. Through precise mathematical formulations and boundary-focused computations, BEM offers a powerful solution to complex FSI challenges in the field of micro elastofluidics.

BEM offers several advantages for FSI in micro elastofluidics. BEM is particularly advantageous for problems defined on unbounded domains, as it only requires discretization of the boundary where the solution is sought. This makes BEM well-suited for problems where the solution behaviour is primarily on the boundary or exterior of the domain, such as in potential flow problems, acoustics, and some electromagnetic problems. BEM potentially requires fewer elements and computational resources compared to volumetric discretization methods, leading to reduced computational effort. However, the boundary element method also has limitations. BEM can face challenges in dealing with internal singularities within the domain, requiring additional techniques or modifications to accurately handle such cases. Furthermore, the accuracy of BEM can cause errors in boundary conditions that may significantly affect the solution. Despite the reduced domain discretization, BEM can become complex and computationally demanding for highly irregular or complex geometries.

In the context of microfluidics, BEM has been utilised to model and analyse fluid-structure interactions. For example, Martinez *et al.* [70] demonstrated the use of BEM for prototyping paper-based microfluidic designs. Li *et al.* [71] also utilised BEM to create paper-based microfluidic devices by plasma treatment, showcasing the method's versatility in creating microfluidic devices. Additionally, Everstine *et al.* [72] developed a coupled finite element/boundary element approach for FSI, demonstrating the capability of BEM in addressing complex FSI.

3.3. Molecular Dynamics Method

Molecular dynamics (MD) simulations are a potent computational method for studying the behaviour of microfluidics at the molecular level. In MD simulations, positions and velocities of individual atoms or molecules are tracked overtime by the numerical integration of Newton's equations of motion, **Figure 8C**. This allows for the investigation of the dynamic behaviour and interactions of the fluid and structure constituents in microfluidic devices and systems.

Theoretically, the MD method includes all reactions and forces happening at the atomistic level and then integrates these effects to the global level and defines the fluid properties and states. For example, a fluid consisting of N interacting atoms or molecules generally represented as particles, each characterised by positions x_i and velocities v_i , where $1 \leq i \leq N$, the Newton equation of motions is as follows [73]:

$$\frac{d}{dt}x_i = v_i \quad (13)$$

$$\frac{d}{dt}v_i = \frac{1}{m_i} \nabla_i V(x_1, \dots, x_N) \quad (14)$$

where; $1 \leq i \leq N$

The individual velocities are derived from Hamiltonian dynamics [74]. The Hamiltonian represents the total energy of the system, encapsulating both kinetic and potential energy components. The Hamiltonian (\mathcal{H}) of a molecular system in MD simulations is defined as the sum of the kinetic energy (T) of the particles and the potential energy (V) arising from their interactions as [74]:

$$\mathcal{H} = T + V = \sum_{i=1}^N \frac{|\vec{p}_i|^2}{2m_i} + V(\vec{r}_1, \vec{r}_2, \dots, \vec{r}_N) \quad (15)$$

where N is the number of particles, \vec{p}_i is the momentum of the i th particle, \vec{r}_i is its position, and m_i is its mass. Further, the momentum \vec{p}_i is related to the velocity v_i of the particle by $\vec{p}_i = m_i v_i$. The potential energy V represents all the interactions between particles. These interactions can be intramolecular (bond stretching, angle bending, dihedral angles) and intermolecular (van der Waals forces, electrostatic forces). The specific form of V depends on the model and the nature of the forces considered, often derived from quantum mechanical calculations or empirical data. Hamiltonian dynamics inherently conserves the total energy, as well as other quantities like linear momentum and angular momentum, assuming no external forces acting on the system.

Due to the nature of being a system of ordinary differential equations, the integration process of **equation (14)** is numerically relatively simple. The ease of numerical integration is a key factor that contributed to the widespread utility and popularity of MD as a valuable simulation method for various problems. However, in scenarios where a fluid spans macroscopic length scales, computational modelling solely with MD is currently unattainable due to the substantial number of particles present in a macroscopic fluid section. Given the impracticality of MD for such scenarios, it is often more convenient to approximate the behaviour of the fluid as a continuum rather than a collection of individual particles. This continuum description can be derived directly from **equation (14)**. Considering the probability density function $f(\{x_i\}, \{v_i\}, t)$ representing the positions and velocities of the N particles. The continuum mass density and velocity fields of the fluid are then defined respectively as [73]:

$$\rho(x, t) = \sum_{k=1}^N m_k \int dx_1, \dots, dx_N dv_1, \dots, dv_N \delta(x - x_k) f(\{x_i\}, \{v_i\}, t) \quad (16)$$

and

$$u(x, t) = \frac{1}{\rho(x, t)} \sum_{k=1}^N m_k \int dx_1, \dots, dx_N dv_1, \dots, dv_N v_k \delta(x - x_k) f(\{x_i\}, \{v_i\}, t) \quad (17)$$

It's important to note here these fields such as mass density, velocity, and pressure are connected to statistical average microscopic densities of these quantities, reflecting a statistical average over a large number of molecules. Therefore, the continuum approximation used in fluid dynamics, thus, can be seen as a moment or mean-field approximation, where macroscopic properties are derived from the averaged effects of microscopic interactions. This approach bridges the gap between molecular-level behaviours captured by MD simulations and the macroscopic descriptions typical of continuum mechanics. The accuracy and reliability of MD simulations depend on the choice of force fields and simulation parameters. Force fields describe the interatomic or intermolecular interactions

and are critical for obtaining accurate results. These forces involve Lennard-Jones potentials for van der Waals forces, Coulombic potentials for electrostatic forces, and specific bonded interactions (stretching, bending, and torsional forces for polymers).

Several works have been performed to study the elastic and viscous properties of the fluid at the micro and nanoscale using MD simulations. For instance, Liu *et al.* [75] conducted MD simulations to investigate the mechanical properties of polymer nanocomposites. The simulation provided insights into the effect of nanoparticle size, concentration, and surface chemistry elastic modulus and viscosity of the composite material. Transport properties and fluid flow behaviour in microfluidics have been studied by MD simulations. For instance, Wang *et al.* [76] used MD simulations to investigate the flow of polymer solutions through microchannels. The authors analysed the effects of polymer concentration, molecular weight, and channel geometry on flow behaviour and observed the formation of elastic instabilities.

MD simulations also enabled the study of behaviour of biological systems. Zhang *et al.* [77] performed MD simulations to investigate the mechanical properties of red blood cells (RBCs) in microchannels. The authors studied the deformation and flow behaviour of RBCs under various conditions and observed the formation of cell-free layers and cell aggregation.

MD simulations can provide valuable insights into the elastic and viscous properties of fluids at the molecular level. They allow for the study of complex phenomena and provide an in-depth understanding of the underlying mechanisms at the molecular scale. However, MD simulations are computationally expensive and limited in terms of system size and simulation time. Therefore, they are frequently paired with other simulation techniques and experimental data.

3.4. Lattice Boltzmann Method

Lattice Boltzmann methods (LBM) have emerged as a powerful numerical technique for studying fluid-structure interactions in microfluidics. LBM describes the statistical behaviour of the particles in a fluid [78]. These methods discretise space and time into a lattice and simulate the movement and interactions of particles on the lattice. One advantage of LBMs is their ability to handle complex geometries and boundary conditions with parallel computing. LBM has been widely used to simulate complex systems such as multiphase fluids [79–81] and biological flows [82–84], and to study fluid-structure interactions [85–88] as well as rheological properties of red blood cells [89]. However, its application in micro elastofluidics remains unexplored, especially for FSI.

Figure 8D illustrates the common lattice structures used in LBM simulations, namely the D2Q9 (two-dimensional with nine velocities) square, D3Q19 (three-dimensional with 19 velocities), and D3Q27 (three-dimensional with 27 velocity vectors) cube lattice configurations. These structures are frequently employed in LBM simulations [90]. We use the D2Q9 model as an illustration to simplify the discussion of LBM. Similar information regarding other models is readily accessible in the existing literature.

While considering the D2Q9 model, the following are the nine velocity vectors of lattice points [90].

$$\mathbf{c}_i = \begin{cases} 0 & \\ \left(\cos \frac{i-1}{2} \pi, \sin \frac{i-1}{2} \pi \right) \frac{\Delta x}{\Delta t} & , i = 1 - 4 \\ \sqrt{2} \left(\cos \frac{2i-9}{4} \pi, \sin \frac{2i-1}{4} \pi \right) \frac{\Delta x}{\Delta t} & , i = 5 - 8 \end{cases} \quad (18)$$

The main variable in LBM represents the fraction of particles travelling with lattice velocity, within lattice site x and time t . For instance, f_0 represents particles at rest as $c_0 = (0,0)$. Following a time step Δt , $f_i(x,t)$ moves to an adjacent lattice site $x + c_0 \Delta t$ along the lattice velocity c_i , a process known as streaming or propagation.

At this site, collisions occur among particles moving from different directions, altering the original particle numbers in each direction. As an outcome, another propagation system is started when a fresh set of density distributions with different lattice velocities emerge from the collision site. This sequence of propagation and collision processes recurs iteratively in LBM simulations until a satisfactory result is obtained.

The above dynamic process is mathematically formalised through the Lattice Boltzmann Equation (LBE) as [91]:

$$f_i(x + c_i \Delta t, t + \Delta t) - f_i(x, t) = \Omega_i(f) \quad (19)$$

In this context, collision operator Ω_i is in charge of figuring out that distribution changes when the collision occurs. The propagation process previously explained is represented on the left-hand side of the equation using Bhathagar–Gross–Krook (BGK) single-time approximation we can approximate the collision operator which is an important simplification of LBM. Initially introduced for the Boltzmann equation within continuum kinetic theory by Bhatnagar *et al.* [92], the lattice BGK (LBGK) equation can thus be expressed as:

$$f_i(x + c_i \Delta t, t + \Delta t) - f_i(x, t) = -\frac{f_i(x, t) - f_i^{eq}(x, t)}{\tau} \quad (20)$$

where collision operator Ω_i is defined as:

$$\Omega_i = -\frac{f_i^{neq}}{\tau} \quad (21)$$

where τ is BGK single relaxation time and f_i^{neq} is a non-equilibrium population that can be expressed as:

$$f_i^{neq} = f_i(x, t) - f_i^{eq}(x, t), \quad (22)$$

where $f_i^{eq}(x, t)$ is discretised population at an equilibrium state at any point x and time t , that can be calculated by discretization of the Maxwell–Boltzmann equilibrium distribution [93] by the following polynomial:

$$f_i^{eq} = \rho \omega_i \left[1 + \frac{u \cdot c_i}{c_s^2} + \frac{1}{2} \left(\frac{u \cdot c_i}{c_s^2} \right)^2 - \frac{u \cdot u}{2c_s^2} \right] \quad (23)$$

From the density distribution across the lattice, fluid density ρ and velocity u can be calculated as:

$$\rho = \sum_i f_i \quad (24)$$

and

$$\rho u = \sum_i f_i c_i \quad (25)$$

Here, c_s is the lattice speed of sound and ω_i is the lattice weight factor that depends on the lattice structure. For D2Q9 model, $\omega_0 = 4/9$, $\omega_{1-4} = 1/9$, $\omega_{5-8} = 1/36$ and $c_s^2 = \Delta x^2 / 3\Delta t^2$. By the Chapman-Enskog expansion continuum macroscopic properties and momentum equation (Navier-Stokes equation (2)) can be obtained from the above LBM discretised dynamics [94].

In BGK single relaxation time, the kinematic viscosity ν and dynamic viscosity μ can be calculated as:

$$\nu = (\tau - \frac{1}{2}) c_s^2 \Delta t \quad (26)$$

and

$$\mu = c_s^2 \rho (\tau - \frac{\Delta t}{2}) \quad (27)$$

3.4.1. Force Application in FSI

Many microfluidic systems are subject to internal or external forces, including gravity [95], electric or magnetic forces [96,97], centrifugal force [98], and fluid-particle interaction [99]. The impact of a body force is conceptualised physically as the addition of momentum to the field. Therefore, a force component post-collision [100] is typically included in the LBE to account for this forcing influence on fluid dynamics. External forces are usually incorporated in the LB algorithm as a source term S_i and a change to the equilibrium velocity u^{eq} as follows [101]:

$$f_i(x + c_i \Delta t, t + \Delta t) - f_i(x, t) = \Omega_i \Delta t + S_i \Delta t \quad (28)$$

also

$$f_i(x + c_i \Delta t, t + \Delta t) - f_i(x, t) = -\frac{f_i(x, t) - f_i^{eq}(x, t)}{\tau} + S_i \Delta t \quad (29)$$

The expression of S_i and u^{eq} are not the same for all types of forcing schemes, for a physical force density F , multiple forcing schemes exist. This paper does not seek to cover all available forcing approaches. Instead, we highlight here the two prevalent forcing approaches: Guo [102] and Shan-Chen [103].

In the Guo scheme, force source term S_i is expressed as:

$$S_i = \omega_i \left(1 - \frac{\Delta t}{2\tau} \right) \left(\frac{c_i \cdot u}{c_s^2} + \frac{u \cdot c_i}{c_s^4} \right) \cdot F \quad (30)$$

And equilibrium velocity becomes:

$$u^{eq} = \frac{1}{\rho} \sum_i f_i c_i + \frac{F \Delta t}{2\rho} \quad (31)$$

In the Shan-Chen scheme, the source term is zero $S_i = 0$, but the equilibrium velocity changes including the effect of external force:

$$u^{eq} = \frac{1}{\rho} \sum_i f_i c_i + \frac{\tau F}{\rho} \quad (32)$$

These adjustments exhibit an increase in fluid momentum at a lattice node by $F \Delta t$ per time step while preserving the fluid density. The above schemes can be used in simulating fully coupled fluid-structure interaction or one-way fluid-structure interaction by applying external force through the Lattice-Boltzmann method [102,104–106].

3.4.2. Boundary Conditions

In LBM, substantial efforts are required to devise accurate and efficient boundary effects [107–109]. Most of the time, periodic boundary conditions are necessary at the inlet and outlet for simulating the fluid dynamics of repetitive or continuous systems. The periodic boundary conditions ensure consistent flow and properties by mimicking an infinite system. These conditions are particularly useful in reducing computational complexity and avoiding boundary-induced errors, making them vital for accurate and stable simulations.

In micro elastofluidics, where the flexible nature of materials poses unique challenges, wall-fluid boundary conditions are critical for accurately modelling fluid dynamics. Techniques such as Simple Bounce Back (SBB) [110] and Mid-Grid Bounce-Back [111] are used for rigid structures, while Modified Bounce-Back [110] and Immersed Body Method [112] are applied to flexible channels and deformable particles to effectively simulate flow interactions at boundaries. In SBB, the particle simply reflecting bounced backward to the initial node x_f in the opposite direction. After collision population f_i^* moving from a fluid node x_f to a solid node x_s in the SBB method is shown in **Figure 8E(i)**. The bounce-back population both in bounce back method or mid-grid bounce back method can be expressed as [111]:

$$f_i(x_f, t + \Delta t) = f_i^*(x_f, t) \quad (33)$$

In this approach, the no-slip condition can achieve second-order accuracy when the physical wall is straight, parallel with one of the main lattice axes, and positioned midway between x_f and x_s .

For managing curved boundaries, the interpolated/extrapolated bounce-back method is the most popular enhancement that is applicable to the SBB technique [113,114]. This method considers the separation between the actual wall position and the lattice nodes as shown in **Figure 8E(ii)**. In this case, following the collision step, a hypothetical distribution is presumed to depart from the solid node x_s and traverse toward the fluid node x_f along a lattice direction and approximated as [115]:

$$f_i^*(x_s) = (1 - X)f_i^*(x_f) + Xf_i^*(x_b) \quad (34)$$

where the two terms on the right-hand side are the interpolation between x_f and x_b with X the contributing factor as defined by Filippova *et al.* [115].

In micro elastofluidics, addressing moving boundary conditions is important when dealing with dynamic interfaces or deformable structures. As discussed before, methods like modified bounce-back and immersed boundary are used for modelling the dynamic interactions between fluids and deformable structures. In the former method, the bounce-back technique is modified to consider scenarios involving moving boundaries, whether it's due to externally imposed motion or in effect of a fully coupled fluid-structure interaction. The momentum transfer at a moving boundary is captured by incorporating a correction term in SBB introduced by Ladd *et al.* [110] as:

$$f_i(x_f, t + \Delta t) = f_i^*(x_f, t) - \frac{2\omega_i \rho_w c_i u_w}{c_s^2} \quad (35)$$

where u_w and ρ_w are the wall velocity and density respectively. For the Interpolated Bounce-Back (IBB) method, the correction term needs to be implemented on the segment of the population after the collision that moves into the wall boundary [116].

3.5. Immersed Body Method in FSI

Originally intended for deformable membranes inside a flow field, the Immersed Boundary Method (IBM) was created by Peskin [112]. An integral relationship can be used to calculate the membrane force from membrane deformation. Membrane forces are transferred to the local fluid as part of fluid-membrane interactions and the membrane configuration was updated in response to the local flow velocity. This method has the advantage of avoiding problems related to shifting boundaries by allowing numerical techniques to solve fluid flow on a fixed, regular Eulerian mesh. In microfluidics, the immersed body approach has been effectively combined with a solver for both soft and rigid particles [117–120]. This technique has also been used to investigate the dynamics of RBCs in microcirculation [121,122].

When a fundamental relationship of solid boundaries is not available, alternative relationships must be developed between the desired boundary velocity and the boundary force to stimulate solid particles and moving boundaries in a flow. Many approaches have been proposed. For example, Feng *et al.* [88] propose modelling solid particles as deformable, using a spring force to represent interactions between each particle and a virtual reference point. This approach allows the simulation of how particles elastically respond to displacement, aiding in understanding their behaviour under various stress conditions. Niu *et al.* [123] determined the boundary force through the momentum interchange of particle distributions at the boundary. Dupuis *et al.* [124] used LBM with IBM for modelling the Navier-Stokes **equation (2)**. The boundary force was calculated by comparing the desired boundary velocity with that computed without the boundary force to account for the no-slip boundary condition.

IBM uses the Lagrangian description for the immersed structures and the Eulerian description for the fluid flow. This method takes into account the movement and distortion of immersed bodies while accurately representing fluid behaviour. In order to take into consideration the impact of immersed structures on surrounding fluids, this approach utilises forcing functions. These features allow forces to be transferred from the fluid to the immersed bodies, enabling the fluid to act on the structures and vice versa. A collection of Lagrangian points or markers positioned within the Eulerian grid serves as the representation of immersed boundaries. Interpolation techniques compute the influence of these markers on the surrounding fluid grid as shown in **Figure 8F**.

Methods such as interpolation and projection are employed to transfer information between the Eulerian and Lagrangian domains, ensuring the accurate exchange of forces, velocities, and displacements between the fluid and structures. The typical IBM process involves several key steps.

The first step is interpolating the velocity of fluid $u(X)$ at position x_i of every particle mesh vertex i in **Figure 8F**. The interpolated velocity \dot{x}_i is given by [49]:

$$\dot{x}_i = \Delta x^d \sum_X u(X) \delta(X - x_i) \quad (36)$$

where d is the number of spatial dimensions, Δx is the lattice spacing, δ and is a discrete delta distribution. After interpolating the fluid velocity, the force f_i acting on each vertex i is calculated. For soft particles, the forces resulting from mesh deformation caused by moving vertices, leading to the changing distance $|x_i - x_j|$ over time. Then spread each vertex force f_i on the fluid, treating them as body forces $F(X)$ according to [49]:

$$F(X) = \sum_i f_i \delta(X - x_i) \quad (37)$$

After spreading the force as per **equation (37)**, the method updates the position and orientation of each particle based on the forces acting on it. The position of the vertex can be updated as:

$$x_i(t + \Delta t) = x_i(t) + \dot{x}_i(t) \Delta t \quad (38)$$

The shape of the discrete delta distribution $\delta(X - x_i)$ is crucial, and a common simplification is using factorised 2D or 3D kernel functions.

For soft particles, the vertex velocity is determined by interpolating fluid velocity. Particle deformation is caused by moving vertices. For rigid particles, challenges involve satisfying rigidity conditions and no-slip conditions simultaneously. Various IBM algorithms for rigid particles exist, such as direct-forcing, implicit IB, and multi-direct-forcing methods.

When a system features symmetric or periodic spatial characteristics, symmetric or periodic boundary conditions can be effectively applied to reduce the computational domain and enhance efficiency. These conditions are particularly well-suited to simulations using IBM due to their adaptability with particle-based models. For periodic boundaries, particles that exit the domain on

one side are reintroduced from the opposite side, effectively simulating an infinitely extended horizontal domain with identical repeating units. Additionally, to implement a pressure gradient in a channel, the periodic boundary condition can be modified to account for a pressure (density) variation between the domain’s inlet and outlet [109].

The two main approaches for flow in geometries with streamwise periodic boundary conditions are: (i) imposing pressure drop Δp on the periodic boundary condition and (ii) a body force \mathbf{F} . The previous approach, which can be substituted by a constant body force $\mathbf{F} = \Delta p$ works well in straight channels with an effective constant pressure gradient. It is often preferable to apply an overall pressure drop Δp between the inlet and outlet for other geometries. Then taking into consideration any pressure variation brought on the particles, the LB algorithm adjusts for the proper pressure field inside the domain. Periodic boundaries are conceptually simple, but they have some difficulties as well. Controlling long-range particle-particle interactions across boundaries is necessary to simulate an infinite number of particles. This frequently involves sensitivity tests of selected channel length [125,126].

Creating more appropriate boundary conditions for complex geometries remains a difficult task. Distortion in the flow field can spread downstream in inertial flows. Any upstream influence is ignored when using a fully formed velocity profile at the inlet, which is not suitable for obtaining accurate results. Further research is required to facilitate practical and accurate LB simulations of microfluidic devices that cannot be approximated with periodically repeating boundary conditions.

Table 1. Summary of Computational Methods and Applications.

Feature	FEM	BEM	MD	LBM	IBM
Basic Principle	Divides problem domain into discrete elements. Solves for field variables.	Reduces dimensionality by focusing on boundaries only. Solves integral equations.	Simulates behaviour of atoms and molecules using Newton's laws of motion.	Simulates fluid dynamics using discrete particle distribution functions on a lattice.	Simulates fluid and structure interaction by embedding the structure in a fluid mesh.
Primary Applications	Structural analysis, micropumps and microvalves.	Acoustic streaming in microfluidics, fluid flow in infinite domains	Biophysics, chemistry, biosensors, and drug delivery systems.	Droplet Generation, fluid flow in complex geometries, multiphase and multicomponent flows	Complex fluid-structure interactions, cardiovascular simulations, biological flows.
Computational Domain	Volumetric domain requires discretization of the entire region.	Surface-based, requires discretization of the boundary only.	Atomic or molecular scale simulates each particle individually.	Volumetric, based on a fixed grid of discrete points.	Hybrid approach combines a fluid mesh with structures that do not conform to the mesh.
Strengths	Flexible, can handle complex geometries and multiphysics problems.	Less discretization is needed, faster for problems with small boundaries.	Provides detailed molecular-level information.	Efficient for complex boundary conditions and scalable for large systems.	Efficiently handles interaction between fluid and immersed structures without requiring mesh conformity.

Table 1. Continued.

Feature	FEM	BEM	MD	LBM	IBM
Weaknesses	Can be computationally intensive, especially for large or complex domains.	Limited to problems where boundary definition is clear and sufficient.	Computationally intensive, limited to relatively small system sizes or short time scales.	Accuracy depends on lattice resolution, and handling complex physics can be challenging.	Can suffer from accuracy issues near the boundary between the fluid and the structure.
Mesh Dependency	Highly mesh-dependent, solution accuracy increases with finer mesh.	Only boundary needs meshing, reducing overall mesh dependency.	No traditional mesh, but particle density and interaction range are crucial.	Mesh (lattice) dependent, though generally less sensitive than FEM.	Mesh of the fluid needs to be fine enough to accurately capture boundary layer phenomena.
Typical Solvers	Direct solvers, iterative solvers.	Boundary integral methods, direct solvers.	Verlet integration, velocity Verlet, leapfrog methods.	Collision and streaming operators, often using BGK approximation.	Direct forcing methods, Lagrangian-Eulerian solvers.
Software Examples	ANSYS, Abaqus, COMSOL Multiphysics.	ANSYS, BEASY, Altair AcuSolve.	LAMMPS, GROMACS, NAMD.	Palabos, OpenLB, LBMflow.).	IBAMR, immersed boundary (MATLAB)

4. Applications

Computational FSI methods are pivotal in micro elastofluidics, enhancing the design and functionality of devices such as microvalves, micropumps, and micromixers. These techniques enable precise modelling of fluid and structural dynamics, critical for devices that control and manipulate fluid flow at the microscale. FSI is also instrumental in biomedical applications, including cell separation and particle manipulation. Additionally, in cardiovascular applications, FSI helps to develop devices that match the biomechanical properties of blood and vascular tissues, significantly improving the intended therapeutic purpose. This underscores the integral role of FSI in advancing micro elastofluidic technology across various scientific and medical fields.

4.1. Microvalves and Micropumps

Microvalves and micropumps are the typical microfluidic components with strong FSI. FSI dictates how flexible membranes and channels within these devices respond to fluid pressure, ultimately shaping their ability to regulate and deliver tiny volumes of liquid in lab-on-a-chip and drug-delivery devices. Much work has been done in analysing the intricate interplay between fluid forces and deformations of flexible structures. Researchers have proposed designs of microvalves and micropumps that achieve unparalleled precision in flow control.

Among the different types of microvalves, elastomeric membrane [127] microvalves are a prime example of where FSI plays a critical role [128]. The core principle behind these valves is the deformation of a flexible membrane in response to fluid pressure [129]. Active valves often utilise external actuation through FSI for precise flow control. Various actuation mechanisms have been proposed [130–134]. Passive valves harness flow forces through FSI to achieve remarkable self-regulation [135–137]. In a passive microvalve, the fluid pressure deforms the membrane, which in turn alters the flow resistance. This dynamic interplay between the fluid and the membrane allows the valve to maintain a constant flow rate over a specific pressure range.

Numerous models for passive check valves and passive regulating valves have been proposed. For instance, Nguyen *et al.* [138] utilised FSI to study passive valves and proposed models for ortho-

planar micro check valves for incorporation in polymeric microdevices, **Figure 9A**. These check valves efficiently prevent backflow and require an inlet pressure of less than 1 kPa to open. Ortho-planar designs provide enhanced sealing performance, thanks to their parallel out-of-plane motion. Later Kartalov *et al.* [139] proposed a PDMS push-up valve utilising the pressure drop along the channel length and performed FSI simulation to investigate the flow rate and threshold pressure, **Figure 9B**. This model maintained a constant flow rate of 0.033 mL/min with a threshold pressure of 103 kPa. Yang *et al.* [140] designed a planar check valve and did an FSI study to model self-adaptive variable resistors to use in microfluidics models, **Figure 9C**. This valve design achieved a relatively high flow rate of 1.2 mL/min with a threshold pressure of 100 kPa. In addition, Doh *et al.* [141] developed a passive parallel membrane valve designed for low-threshold pressure operation using the concept of FSI, **Figure 9D**. The valve consists of two control channels, two vertically oriented membranes, and a single fluidic channel. The autonomous deflection of the membranes within the microchannel enables the valve to achieve flow regulation at a pressure as low as 15 kPa. Moreover, Zhang *et al.* [142] utilised FSI on flow regulation in microfluidic environments and developed a unique parallel membrane valve featuring a stacked five-layer architecture, **Figure 9E**. This design, with two horizontal membranes enclosing a fluidic channel and sandwiched between control channels, achieved a remarkable flow rate of 2.79 mL/min with a low 10 kPa threshold pressure. Zhang *et al.* [137] achieved low threshold pressure in microfluidic high throughput delivery systems and designed a passive valve for stable flow control. The valve utilises an ellipsoid control chamber and a dual micro-hole elastic membrane, **Figure 9F**. Membrane deflection in response to pressurised flow through the micro-holes dynamically modifies the control chamber's resistance. This self-regulating mechanism maintains a constant flow rate regardless of inlet pressure changes.

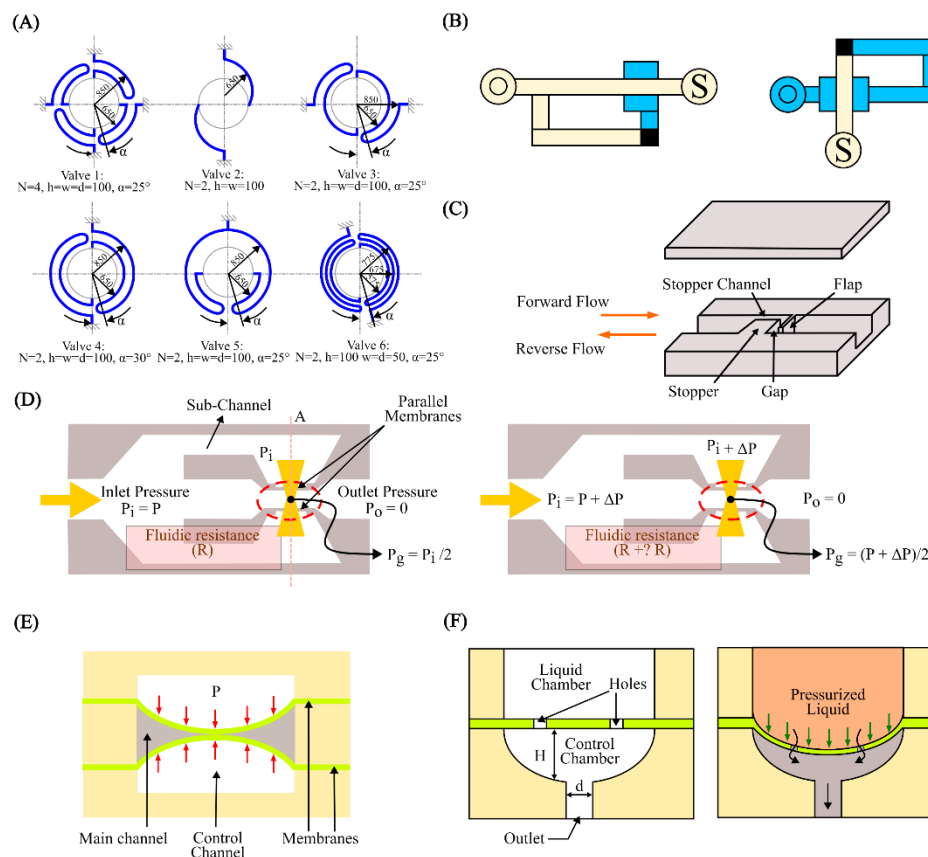


Figure 9. Microvalves and micropumps. Microvalves and micropumps. (A) Ortho-planar micro check valves with different stiffness; (B) Poiseuille Law pressure drop self-regulating valve; (C) Self-adaptive planar check valve with flexible cantilever flap; (D) Parallel membrane with low threshold pressure, self-regulating valve; (E) Stacked parallel membrane with low threshold pressure, regulating valve; (F) Ellipsoid control chamber auto-regulating valve.

Micropump is another crucial component of many microfluidic systems. Since their invention, micropumps have seen significant advancements, offering advantages such as compact size, portability, energy efficiency, wide range of flow rate, affordability, and potential for integration with other microfluidic components. Micropumps are typically constructed using Micro-electromechanical Systems (MEMS) techniques on biocompatible materials such as silicon, glass, or various polymers (such as Polymethyl Methacrylate (PMMA), PDMS, or SU-8 photoresist) [143,144]. Micropumps fall into two broad categories: (i) mechanical, using moving parts like diaphragms and valves, and (ii) non-mechanical which manipulates fluid flow through hydrodynamic [145], electroosmotic [146], or electrowetting [147] forces. In mechanical micropumps, fluid flow is pressurised by an external force i.e. piezoelectric (PZT), electromagnetic (EM), electrostatic, and thermo-pneumatic, applied to either fixed flexible membranes or moving structures. This force transfer to the fluid occurs through fluid-structure interaction. Much work has been done in harnessing and manipulating the pumping function on the micro-scale through FSI. Wang *et al.* [148] proposed a piezoelectric micropump utilising fixed-end PDMS valves with integrated compressible space. This micropump utilises a resonantly driven membrane actuator, two fixed-end PDMS check valves for stability and reduced leakage, and strategically placed compressible spaces, **Figure 10A**.

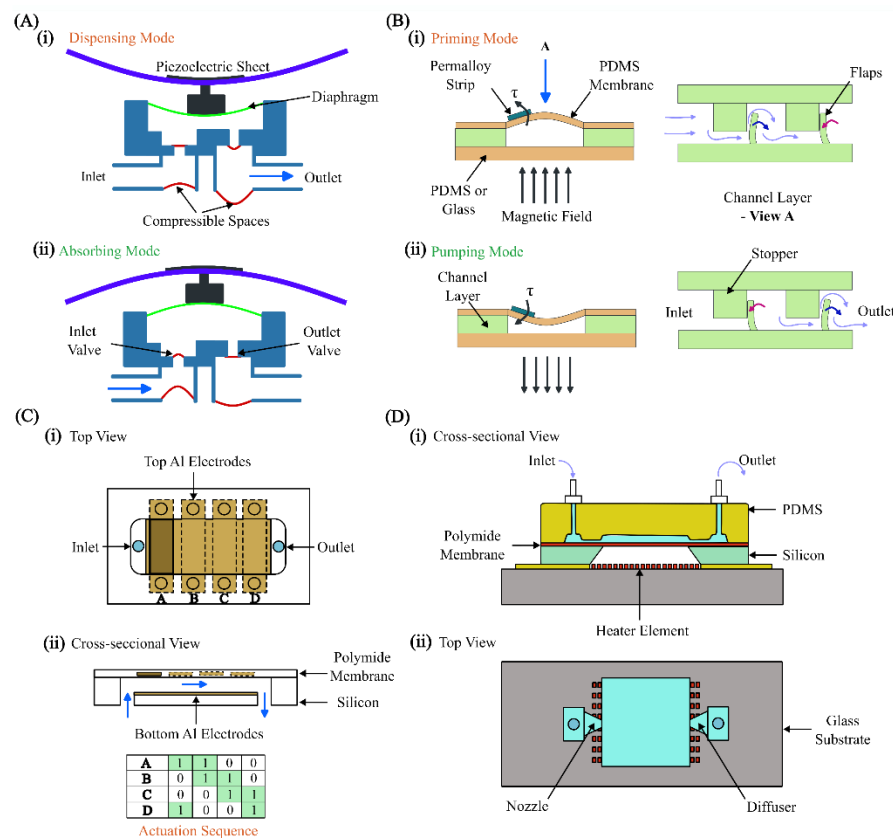


Figure 10. Pumping schemes. (A) Piezoelectric micropump utilizing fixed-end PDMS valves with integrated compressible space; (B) Magnetically actuated membrane micropump with in-plane check valves; (C) Electrostatically actuated micropump utilizing four electrodes to induce peristaltic motion; (D) Thermo-pneumatic micropump with a thin polyimide membrane actuator.

Piezoelectric actuator deforms the pump membrane. This deformation of the membrane affects the fluid inside the pump by changing the space it occupies, which increases or decreases the pressure. Essentially, as the membrane changes shape, it pushes on the fluid, helping to move it through the system. The micropump design relies on two key interactions: (i) electromechanical interaction, where the piezoelectric sheet converts electric signals into movement of the beam, and (ii) fluid-solid interaction, where the pump diaphragm interacts with the working fluid. An alternating voltage causes the beam to deform, driving the membrane and thus the fluid flow.

Simultaneously, the fluid resists the movement of the membrane. The reported micropump delivers a maximum flow rate of 105 mL/min and a maximum back pressure of 23 kPa under a 400 V sinusoidal voltage at 490 Hz. Maximum power consumption at zero back pressure is approximately 42 mW.

Ni *et al.* [149] introduced a magnetic micropump utilising FSI for easy fabrication and seamless integration into other microfluidic systems. The device features in-plane check valves for flow control and a magnetically actuated membrane, **Figure 10B**. The deformable elastic membrane then interacts with the flowing fluid and in turn, pressurises the fluid. Since actuation is controlled directly by an external magnetic field, enabling efficient wireless operation is ideal for various applications. Experimental results indicate that the micropump can deliver 0.15 $\mu\text{L}/\text{min}$ at 2 Hz, offering 1 nL per stroke resolution, and works against 550 Pa backpressure.

Moreover, Lee *et al.* [150] fabricated an electrostatically actuated micropump incorporating FSI, utilising four electrodes to induce peristaltic motion, **Figure 10C**. In this study, the micropump makes use of electrostatic force to create bidirectional peristaltic motion. Its unique design features a single deformable membrane with four movable polyimide electrodes hence eliminating the need for valves. Actuation signals cause the membrane to bend in small, sequential steps, which increases the pressure of the fluid in stages. This action splits a single chamber into two, three, or four separate sections, allowing for controlled movement of the fluid within the device. Experiments showed, optimising the actuation signal dramatically increased the flow rate. With a basic signal, the pump achieved 38 $\mu\text{L}/\text{min}$, but an optimised signal boosted this to 136 $\mu\text{L}/\text{min}$ (both at 90 V and 15 Hz). This represents a 3.6-fold improvement. Hamid *et al.* [151] modelled a cost-effective thermo-pneumatic micropump with a thin polyimide membrane actuator, **Figure 10D**. The model includes a microheater, thermal cavity, and planar valve. This thermo-pneumatic micropump utilises thermal air expansion within a chamber to actuate a thin polyimide membrane. The membrane movement then interacts with the fluid and hence creates pressure fluctuations accordingly. This device effectively controls fluid on the picolitre to nanolitre scale, making it suitable for applications such as artificial kidneys and drug delivery systems, and is both simple and economical to fabricate.

4.2. Cell and Particle Manipulation

Cell sorting is a laboratory technique for isolating a specific cell type from a mixed population. Isolation criteria include physical parameters (size, morphology), cell viability, and the presence of specific intracellular or extracellular proteins [152]. Purified cells obtained through sorting are essential tools for research, diagnostic procedures, and cell-based therapies. Cell sorting encompasses a broad range of established techniques, employing both active and passive mechanisms [153]. Active sorting utilises external fields (electric, acoustic, magnetic, or optical) to manipulate cell trajectories. Passive systems primarily leverage inertial forces, filtration, and cell-surface adhesion for purification. Understanding FSI in both cell-fluid and fluid-channel interactions is crucial for optimizing and designing cell sorting devices. Extensive experimental works have been conducted to utilise FSI phenomena for cell sorting and manipulation. However, numerical simulations are vital to fully comprehend these FSI phenomena. Numerical modelling of cell dynamics complements experimental approaches, enabling the in-depth study of fluid-particle interactions. Accurately simulating these dynamic processes presents challenges due to the complexity of FSI coupling, cell mechanics, and the computational cost of simulating cell-cell interactions at scale.

Sun *et al.* [154] developed an LBM model to simulate blood flow in realistic microvascular networks and the separation of different types of cells, **Figure 11A**. This approach allows for the detailed analysis of FSI between blood cells and the vessel wall. This model treated blood as a suspension of particles (red blood cells [RBCs] and white blood cells [WBCs]) within the plasma, explicitly incorporating cell-cell and cell-wall interactions. The LBM approach allows for simulating RBC and WBC interactions as the cells flow through a microvascular network. This approach enables (i) quantification of forces exerted between RBCs and WBCs, tracking of trajectories of individual cells, (ii) analysis of pressure variations within the network due to cellular traffic, and (iii) the evaluation of forces experienced by the vessel walls at any location. Simulations demonstrate that

vessel curvature and junctions increase the apparent viscosity and induce stress perturbations near stagnation points. The results suggested a potential link to atherogenesis at stagnation points and may also significantly influence our understanding of endothelial biology and its role in atherosclerosis formation.

Mao *et al.* [155] conducted computational modelling of particle sorting, specifically addressing FSI, for high-throughput hydrodynamic size-based sorting of solid microparticles in microchannels, **Figure 11C(i)**. With this model, high-resolution separation was achieved by combining cross-stream inertial migration of particles with circulatory flows induced by periodic diagonal ridges on opposite channel walls. A hybrid approach was employed to model the multi-component system of a fluid-filled ridged microchannel and various-sized solid particles. This approach integrates LBM for fluid dynamics with a lattice spring model (LSM) for modelling solids. FSI is captured through appropriate boundary conditions at the solid-fluid interface. Simulations proved to be crucial for designing the ridged microchannel. Optimization for separating neutrally buoyant microparticles by size relied heavily on understanding the complex FSI within a microchannel. **Figure 11C(ii)** shows the results of this study. The geometry of the microchannel induces unique fluid flow patterns, and the resulting FSI between these patterns and the particles is the key to high-resolution separation.

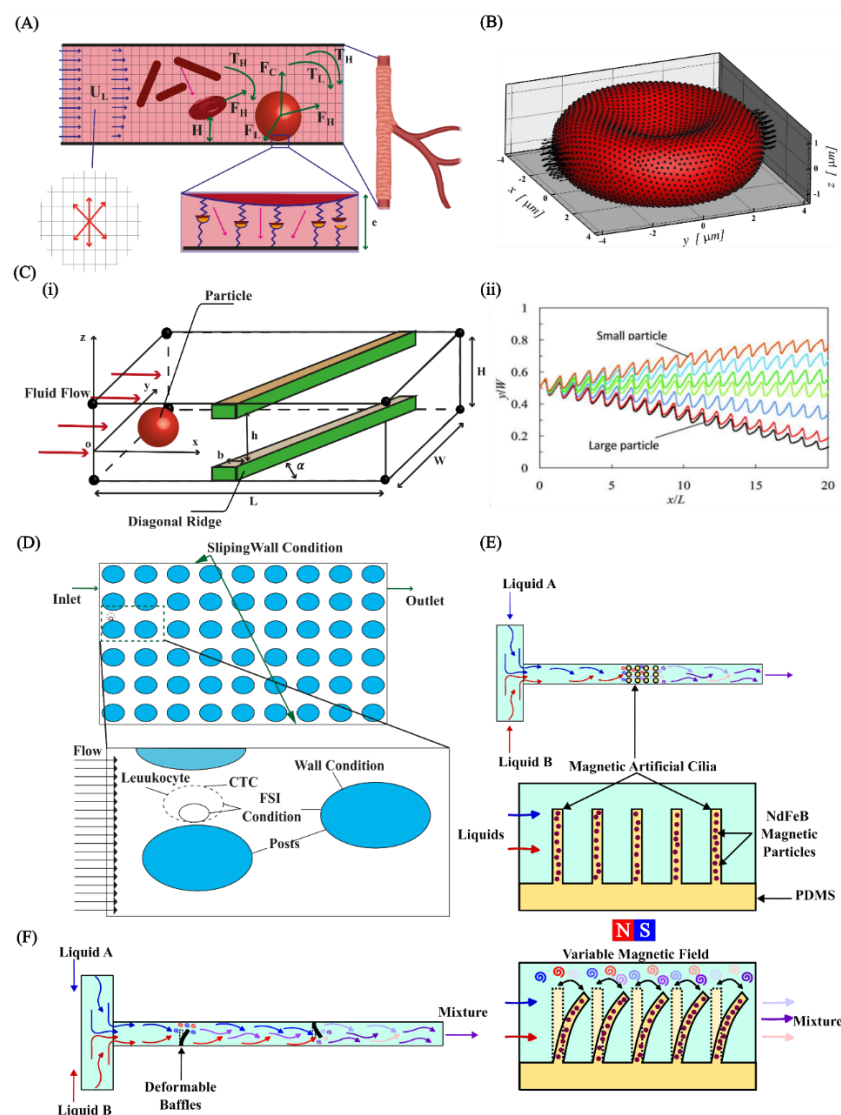


Figure 11. Cell separation and micromixers. (A) Illustration of considering RBC and WBC as suspended particles in plasma to capture fluid-particle and fluid-wall interactions; (B) RBC discretisation to investigate the change in deformability of cells caused by malaria parasites. reproduced with permission from Hosseini *et al.* [156]; (C)(i) Setup for particle sorting in

microchannels, (ii) Particle separation. reproduced with permission from Mao *et al.* [155]; (D) DLD device for separating CTCs within blood stream; (E) Mixing with magnetic actuated artificial cilia; (F) Passive mixing with flexible baffles.

Khodaei *et al.* [157] carried out a numerical FSI study of fluid-particle interaction in a deterministic lateral displacement (DLD) microfluidic device for effective separation of circulating tumor cells (CTC) in bloodstreams. Numerical simulations, incorporating FSI using FEM to model deformable cell behaviour, guide the design of a typical DLD array for separating CTCs and leukocytes (white blood cells) under various flow conditions. **Figure 11D** illustrates the discretization of this method. This study focused on how coupled FSI phenomena, specifically related to flow conditions, stress, and cell deformability impact cell separation in DLD devices. This model provides essential data for optimising DLD devices, enhancing efficiency, and protecting cell viability. The model quantifies the cellular stress experienced during separation and maps the distribution of effective stress at peak deformation.

FSI also plays a fundamental role in accurately simulating cell deformations within a complex environment. Cells are not rigid bodies and respond dynamically to the fluid forces surrounding them. These forces can cause cells to stretch, compress, and change shape. In turn, deformed cells alter the flow field around them. FSI models are essential for capturing this intricate interplay. FSI simulation provides realistic predictions of how cells deform under various conditions. This has far-reaching implications in biomedical research, understanding disease processes where cell deformation plays a role. For instance, Hosseini *et al.* [156] carried out FSI analysis on RBCs and investigated the change in deformability of cells caused by malaria parasites. Numerical simulations incorporating FSI were employed to investigate this phenomenon. The cell membrane was represented as a collection of interconnected, elastic particles, **Figure 11B**. The cytosol is modelled as a Newtonian fluid using smoothed particle hydrodynamic techniques (SPH). More importantly, the malaria parasite was treated as a rigid structure, capturing its influence on the overall behaviour of the cells. Healthy RBCs are remarkably flexible, but the presence of the rigid malaria parasite within the cell significantly increases its stiffness. In response to the fluid forces present in the bloodstream, the deformability of infected cells declines. These findings underscore the potential of using cell deformability as a diagnostic marker and highlight the value of FSI simulation in understanding disease-induced cellular changes.

4.3. Micromixers

Mixing fluids in the microscale presents unique challenges and opportunities. Due to the dominance of laminar flow and the lack of turbulence in the microscale, traditional mixing strategies often become ineffective. This challenge has spurred the development of innovative microfluidic mixing approaches, relying on strategies such as chaotic advection, diffusion enhancement, or the integration of active micromixers. Micromixers are broadly categorised as active and passive types [158]. Active micromixers enhance mixing by introducing external perturbations that disrupt the typically laminar flow regime. Methods include pressure-driven actuation (e.g., pulsatile flows), electrokinetic manipulation (e.g., electroosmotic flow), magnetic actuation (e.g., ferrofluid mixing), or acoustic streaming [159–165]. These techniques offer rapid mixing, tunability, and adaptability, but come with increasing system complexity. In contrast, passive micromixers rely on microchannel geometry to promote mixing. Complex channel geometries induce chaotic advection, increasing interfacial contact area through lamination, splitting, or droplets [166–171]. Passive mixers excel in simplicity, cost-effectiveness, and minimal sample perturbation, but may have longer mixing times and less adaptability than their active counterparts.

FSI plays a vital role in both active and passive micromixers. In active micromixers based on FSI, flexible elements interact with the fluid flow, creating complex patterns that disrupt the laminar flow for fast and efficient mixing. This FSI approach allows for customised flow control, works with various fluids, and potentially uses less power than other active mixing methods. Examples include employing deformable membranes to create chaotic advection or integrating oscillating

microstructures to induce localised mixing zones. While less common than active FSI micromixers, passive designs can also exploit FSI to enhance mixing. These mixers often incorporate flexible or deformable elements within the microchannel that respond to the inherent fluid forces. Examples include flexible micro-posts that sway in response to flow, membranes that deform under pressure, and integrated microvalves whose operation is triggered by fluid forces.

Much work has been done in optimising the design of micromixers using FSI-based numerical simulation. For example, Lin *et al.* [172] carried out an FSI analysis for precise flow manipulation in a micromixer using magnetic actuation. The team employed microstructures with embedded magnetic particles (**Figure 11E**). A CFD approach, utilizing FSI modelling, was employed to simulate the flow patterns generated by the actuated structures. The model revealed the impact of different actuation modes on mixing performance. The 'zigzag' pattern proves to be superior in achieving rapid and complete mixing. Further analysis demonstrated how these structures disrupt and blend the flow, with vorticity calculations pinpointing regions of high vorticity in the flow field. The enhanced vorticity strongly correlates with improved mixing. The study features the power of combining experimental and numerical analyses to understand the FSI mechanisms responsible for effective flow mixing. These findings hold significant value for designing future high-performance micromixers, where speed and thorough mixing are essential. Moreover, Talebjedi *et al.* [173] exploit the FSI phenomenon in passive micromixers using flexible baffles, **Figure 11F**. This research explores the use of deformable baffles in the mixing process, aiming to improve performance compared to traditional rigid baffles. Modelling the FSI provides insight into how deformable baffles change shape under fluid pressure, and how this affects flow. The results show a significant reduction in pressure drop with deformable baffles, indicating less stress on mixed materials. More importantly, this improvement is achieved with only a minor decrease in mixing efficiency as compared to rigid baffles. This suggests that deformable baffles offer a promising way to optimise mixing processes, where reducing stress on the materials being mixed is vital.

4.4. Modelling Cardiovascular Systems

In the realm of micro elastofluidics, computational methods for FSI unlock a deeper understanding of the complex interplay between biological fluids and the flexible tissues they encounter. The complex dynamics of blood flow, coupled with the flexible nature of heart valves and arterial walls, necessitate FSI simulations for a comprehensive analysis of the cardiovascular system. FSI models provide critical insights into heart valve function, including leaflet deformation, flow patterns, and stress distribution, leading to better diagnostics for heart diseases and improved designs for prosthetic replacements [174–178]. Similarly, FSI models applied to artery flow provide insights into the development of arterial diseases like atherosclerosis, uncovering potential risks for aneurysm formation, and contribute to the optimization of medical devices such as stents [179–183].

Heart valves play a critical role in maintaining blood flow direction. Artificial valves are treatment options, but their design and performance require careful analysis. Laha *et al.* [174] investigated bi-leaflet mechanical heart valve dynamics through FSI modelling with Smoothed Particle Hydrodynamics (SPH). **Figure 12** illustrates the schematic model. The team explored a method for simulating a bi-leaflet heart valve using an SPH open-source code. By incorporating FSI, the SPH technique analysed hemodynamic abnormalities associated with valve dysfunction. The study considered normal and abnormal flow behaviour, valve movement under blockage scenarios, and potential risks associated with blockages. The findings demonstrate the effectiveness of this SPH/FSI approach for capturing the dynamic behaviour of bi-leaflet valves. The versatility of this computational model suggests its potential application to more complex cardiovascular problems.

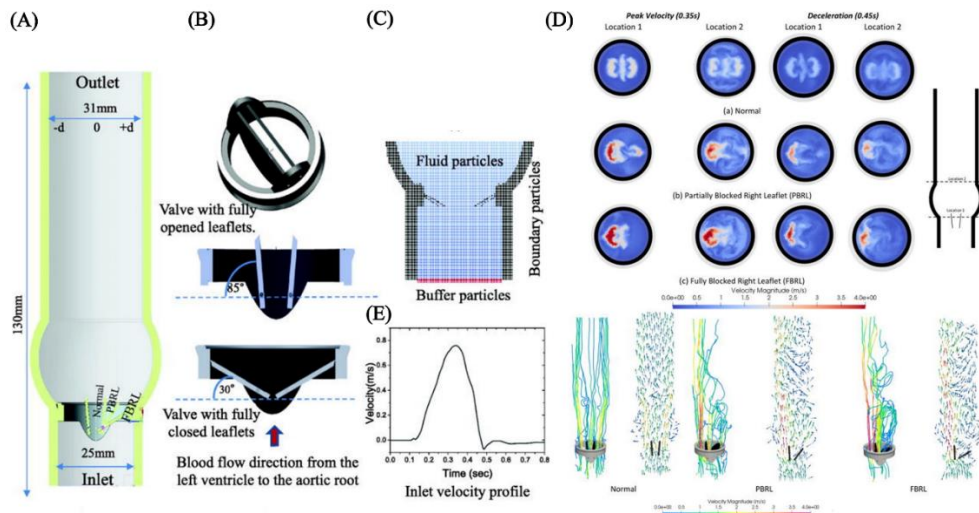


Figure 12. Bi-leaflet mechanical heart valve dynamics through FSI Modelling with Smoothed Particle Hydrodynamics (SPH); (A) Illustration of mechanical heart valve; (B) Opening and closing position of valve; (C) Illustration of smoothed particles for simulation; (D) Inlet velocity profile to mimic the real pulse; (E) Simulation results. reproduced with permission from Laha *et al.* [174].

Sodhani *et al.* [175] carried out an FSI study on an artificial aortic heart valve that was reinforced with textile. In this study, an in-silico FSI model was developed using the immersed boundary method to mimic the in-vitro experiment. The model assessed the geometric orifice area and flow rate over a single cycle, while also incorporating the material properties of the implant. The model employed fixed boundary conditions for the structural part. This involved fixing the bottom and stitched regions of the device in all directions, preventing movement in those areas. For the fluid domain, transvalvular pressure is incorporated as a boundary condition at the inlet and a zero-pressure condition at the outlet. Transvalvular pressure, measured in the corresponding in-vitro test. **Figure 13** shows the model of the heart valve. The FSI simulation provided valuable insights into device performance i.e. pressure distribution, velocity field, recirculation zones, vortices, and potential leakage points. This work demonstrated the effectiveness of FSI simulations for validating material property determination techniques and predicting the kinematics and flow behaviours of the device.

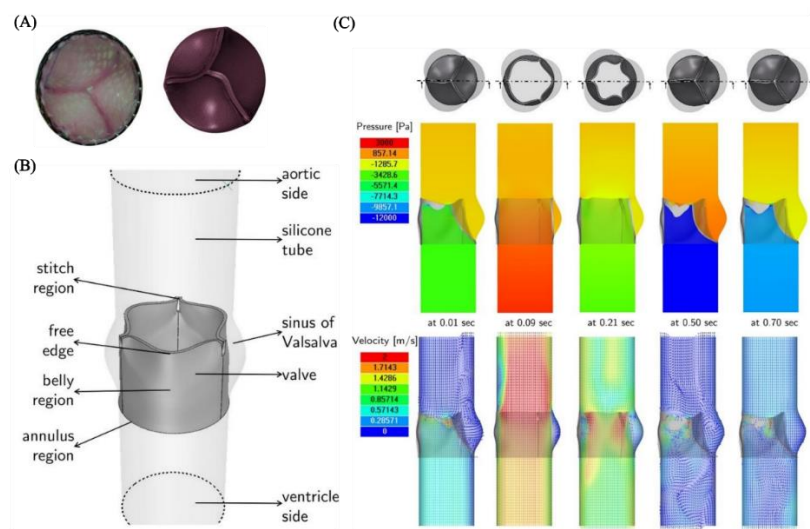


Figure 13. An artificial aortic heart valve. (A) Effect of asymmetry on valve closure (right) and comparison with a similar tex-valve (left); (B) Illustration of test setup for FSI simulations; (C) Simulation results. reproduced with permission from Sodhani *et al.* [175].

Arterial diseases, including atherosclerosis and aneurysms, pose significant health risks due to their potential to cause serious cardiovascular events such as heart attacks and strokes. By accurately simulating the dynamic interactions between blood flow and arterial walls, FSI models provide invaluable insights into mechanical forces that contribute to disease progression. For example, Valente *et al.* [184] carried out the numerical investigation of Ascending Thoracic Aortic Aneurysm (ATAA) through FSI simulations using the open-source software package SimVascular. **Figure 14A** and **14B** illustrate the mesh model and results, respectively. The simulations are based on patient-specific geometric models reconstructed from Computed Tomography (CT) scans. The analysis incorporates specific outlet conditions and temporal flow variations at the model inlet. By assigning prestress, the aorta model accurately reflects the in vivo stress state during the cardiac cycle. The process begins with a CFD analysis on the fluid domain, followed by structural analysis in the solid domain, using the pressures from the CFD phase as boundary conditions. The results from both CFD and Computational Structural Mechanics (CSM) were used as initial conditions for further analysis. The hemodynamic and structural behaviour of ATAA was studied, focusing on the velocity, displacement magnitudes, and wall shear stress distribution during the first cardiac cycle. The results confirm the effectiveness of the simulation in capturing the complex dynamics of ATAA, highlighting its potential for enhanced precision in biomechanical assessments.

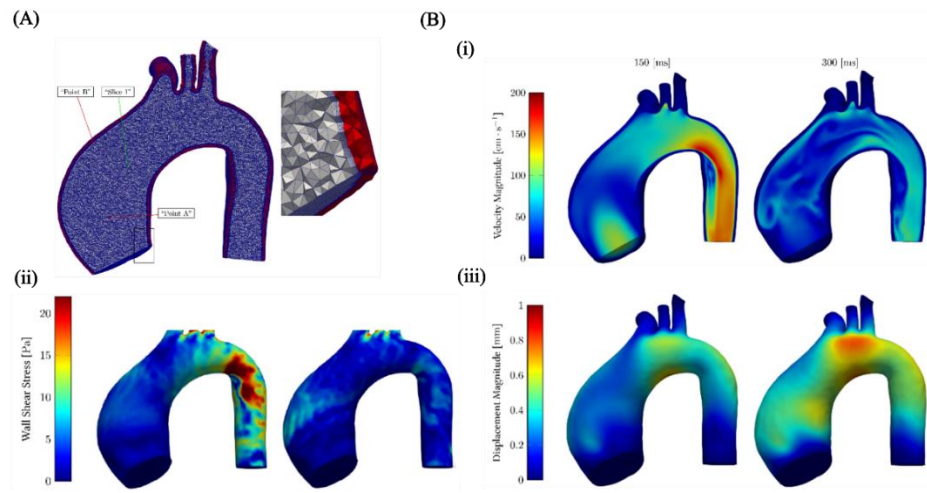


Figure 14. Numerical investigation of Ascending Thoracic Aortic Aneurysm (ATAA) through FSI simulations. (A) Mesh discretisation of patient-specific geometric ascending thoracic aorta model reconstructed from CT scans; (B) Simulations results reproduced with permission from Valente *et al.* [184].

5. Discussion and Future Perspectives

The exploration of FSI in microfluidics using both continuum and particle computational approaches presents a dynamic and promising research area. Computational FSI and the deformable nature of structures in microfluidic devices have created new opportunities for applications across diverse fields, including biotechnology, healthcare, and soft robotics. However, the selection of an appropriate computational method depends heavily on the specific requirements and constraints of the application. Among the computational methods, FEM is highly valued for its robust handling of complex geometries and diverse material properties, making it ideal for scenarios involving significant structural deformations. However, the computational cost makes FEM less efficient for fluid dynamics problems as compared to other methods. BEM offers an advantage for fluid flow around structures by reducing the problem dimensionality since it only requires discretization at the boundaries. The dimension reduction leads to substantial saving of computational cost. However, BEM struggles with non-linear properties and dynamically changing domains. In contrast, LBM is celebrated for its simplicity and efficiency in handling fluid flows and multiphase phenomena, easily integrated with complex boundary conditions. However, coupling LBM effectively with solid

mechanics models remains challenging. MD provides exceptional detail at the molecular level, perfect for analysing microscale interactions within fluids and at fluid-solid interfaces. Yet, its practical application is typically limited to small systems due to the high computational demands. On the other hand, IBM is particularly effective for problems where fluid and structure are dynamically interlinked such as in situations with complex and moving boundaries, when structures within the fluid change position or shape. Despite its versatility, IBM requires careful calibration to accurately capture the dynamics of the fluid-structure interface.

Looking ahead, the potential for computational FSI in micro elastofluidics is vast, with opportunities to combine the strengths of the above methods through hybrid modelling approaches. For instance, integrating LBM's fluid dynamics capabilities with FEM's structural dynamics expertise could yield an approach that leverages the strengths of both LBM and FEM, offering more accurate and comprehensive simulation. As computational resources continue to expand and algorithms evolve, the scope for real-time simulations and enhanced multiscale modelling will broaden, paving the way for more precise and efficient designs.

Real-time simulation capabilities will pave the way for adaptive microfluidic systems that dynamically respond to environmental changes, ideal for biomedical implants and wearable applications. The integration of Artificial Intelligence (AI) will streamline the design process, optimise simulation parameters, and predict system behaviours under diverse conditions, reducing development time and improving device efficacy. Moreover, the focus on sustainable technologies will encourage the integration of biodegradable materials into micro elastofluidic devices, necessitating robust FSI methods to assess their performance. Personalised medicine will also benefit from FSI-optimised devices tailored to individual physiological conditions, optimizing diagnostic and therapeutic outcomes. Overall, these recent advances will significantly enhance the scope and effectiveness of microelastofluidic applications, transforming both technological capabilities and their societal impact.

Author Contributions: N.-T. N. and J. Z. Conceptualization, Supervision, and Project Administration. H. M. M. Formal analysis, Writing-original draft preparation, Visualization. U. R. Editing and Visualization. A. M. Visualization. Q. T. T., J. Z., and N.-T. N. Writing-review & editing. N.-T.N., and J.Z. Funding acquisition. All the authors provided critical feedback and read and approved the manuscript.

Conflicts of Interests: The authors have declared no conflict of interest.

Acknowledgments: The authors acknowledge the support from the Australian Research Council (ARC) Australian Laureate Fellowship (Grant No. FL230100023) and ARC DECRA fellowship (Grant No. DE210100692).

Abbreviations

2D	Two-dimensional
3D	Three-dimensional
AI	Artificial Intelligence
ATAA	Ascending Thoracic Aortic Aneurysm
BEM	Boundary Element Method
BGK	Bhathagar–Gross–Krook
CFD	Computational Fluid Dynamics
CS-FEM	Cell-based Smoothed Finite Element Method
CSM	Computational Structural Mechanics
CT	Computed Tomography
CTCs	Circulating Tumor Cells
DLD	Deterministic Lateral Displacement
EM	Electromagnetic
FEM	Finite Element Method
FSI	Fluid-Structure Interaction
IBM	Immersed Boundary Method
IPMF	Inertial Particle Microfluidics
LBE	Lattice Boltzmann Equation

LBGK	Lattice Bhathagar–Gross–Krook
LBM	Lattice Boltzmann Method
LSM	Lattice Spring Model
MD	Molecular Dynamics
MEMS	Micro-electromechanical Systems
PDEs	Partial Differential Equations
PDMS	Polydimethylsiloxane
PMMA	Polymethyl Methacrylate
PZT	Piezoelectric
RBCs	Red Blood Cells
SBB	Simple Bounce Back
S-FEM	Smoothed Finite Element Methods
SPHs	Smoothed Particle Hydrodynamics
WBCs	White Blood Cells

References

1. Nagrath, S.; Sequist, L.V.; Maheswaran, S.; Bell, D.W.; Irimia, D.; Ulkus, L.; Smith, M.R.; Kwak, E.L.; Digumarthy, S.; Muzikansky, A. Isolation of rare circulating tumour cells in cancer patients by microchip technology. *Nature* **2007**, *450*, 1235-1239.
2. Adams, A.A.; Okagbare, P.I.; Feng, J.; Hupert, M.L.; Patterson, D.; Göttert, J.; McCarley, R.L.; Nikitopoulos, D.; Murphy, M.C.; Soper, S.A. Highly efficient circulating tumor cell isolation from whole blood and label-free enumeration using polymer-based microfluidics with an integrated conductivity sensor. *Journal of the American Chemical Society* **2008**, *130*, 8633-8641.
3. Jiang, J.; Zhao, H.; Shu, W.; Tian, J.; Huang, Y.; Song, Y.; Wang, R.; Li, E.; Slamon, D.; Hou, D. An integrated microfluidic device for rapid and high-sensitivity analysis of circulating tumor cells. *Scientific reports* **2017**, *7*, 42612.
4. Yeo, L.Y.; Chang, H.C.; Chan, P.P.; Friend, J.R. Microfluidic devices for bioapplications. *small* **2011**, *7*, 12-48.
5. Nguyen, N.-T. Micro elastofluidics: elasticity and flexibility for efficient microscale liquid handling. **2020**, *11*, 1004.
6. Kim, H.; Kim, J. A microfluidic-based dynamic microarray system with single-layer pneumatic valves for immobilization and selective retrieval of single microbeads. *Microfluidics and nanofluidics* **2014**, *16*, 623-633.
7. Cha, H.; Fallahi, H.; Dai, Y.; Yuan, D.; An, H.; Nguyen, N.-T.; Zhang, J. Multiphysics microfluidics for cell manipulation and separation: a review. *Lab on a Chip* **2022**, *22*, 423-444.
8. Fallahi, H.; Zhang, J.; Nicholls, J.; Phan, H.-P.; Nguyen, N.-T. Stretchable inertial microfluidic device for tunable particle separation. *Analytical Chemistry* **2020**, *92*, 12473-12480.
9. Kim, B.; Yoo, S.; Kim, Y.J.; Park, J.; Kang, B.; Haam, S.; Kang, S.W.; Kang, K.; Jeong, U. A Strain-Regulated, Refillable Elastic Patch for Controlled Release. *Advanced Materials Interfaces* **2016**, *3*, 1500803.
10. Song, W.; Vasdekis, A.E.; Psaltis, D. Elastomer based tunable optofluidic devices. *Lab on a Chip* **2012**, *12*, 3590-3597.
11. Raj, A.; Halder, R.; Sajeesh, P.; Sen, A. Droplet generation in a microchannel with a controllable deformable wall. *Microfluidics and Nanofluidics* **2016**, *20*, 1-16.
12. Anoop, R.; Sen, A. Capillary flow enhancement in rectangular polymer microchannels with a deformable wall. *Physical Review E* **2015**, *92*, 013024.
13. Li, N.; Hsu, C.H.; Folch, A. Parallel mixing of photolithographically defined nanoliter volumes using elastomeric microvalve arrays. *Electrophoresis* **2005**, *26*, 3758-3764.
14. Madhumitha, R.; Arunkumar, S.; Karthikeyan, K.; Krishnah, S.; Ravichandran, V.; Venkatesan, M. Computational modeling and analysis of fluid structure interaction in micromixers with deformable baffle. *International Journal of Chemical Reactor Engineering* **2017**, *15*, 20160121.
15. Leslie, D.C.; Easley, C.J.; Seker, E.; Karlinsey, J.M.; Utz, M.; Begley, M.R.; Landers, J.P. Frequency-specific flow control in microfluidic circuits with passive elastomeric features. *Nature Physics* **2009**, *5*, 231-235.
16. Lam, E.W.; Cooksey, G.A.; Finlayson, B.A.; Folch, A. Microfluidic circuits with tunable flow resistances. *Applied Physics Letters* **2006**, *89*.
17. Gan, H.Y.; Lam, Y.C.; Nguyen, N.T.; Tam, K.C.; Yang, C. Efficient mixing of viscoelastic fluids in a microchannel at low Reynolds number. *Microfluidics and Nanofluidics* **2007**, *3*, 101-108.

18. Yuan, D.; Zhang, J.; Yan, S.; Pan, C.; Alici, G.; Nguyen, N.-T.; Li, W. Dean-flow-coupled elasto-inertial three-dimensional particle focusing under viscoelastic flow in a straight channel with asymmetrical expansion-contraction cavity arrays. *Biomicrofluidics* **2015**, *9*.
19. Mehboudi, A.; Yeom, J. A one-dimensional model for compressible fluid flows through deformable microchannels. *Physics of Fluids* **2018**, *30*.
20. Whitesides, G.M. The origins and the future of microfluidics. *nature* **2006**, *442*, 368-373.
21. Lötters, J.C.; Olthuis, W.; Veltink, P.H.; Bergveld, P. The mechanical properties of the rubber elastic polymer polydimethylsiloxane for sensor applications. *Journal of micromechanics and microengineering* **1997**, *7*, 145.
22. Xia, Y.; Whitesides, G.M. Soft lithography. *Annual review of materials science* **1998**, *28*, 153-184.
23. McDonald, J.C.; Whitesides, G.M. Poly (dimethylsiloxane) as a material for fabricating microfluidic devices. *Accounts of chemical research* **2002**, *35*, 491-499.
24. Sia, S.K.; Whitesides, G.M. Microfluidic devices fabricated in poly (dimethylsiloxane) for biological studies. *Electrophoresis* **2003**, *24*, 3563-3576.
25. Raj, A.; Sen, A. Flow-induced deformation of compliant microchannels and its effect on pressure-flow characteristics. *Microfluidics and Nanofluidics* **2016**, *20*, 31.
26. Teo, A.J.; Malekpour-galogahi, F.; Sreejith, K.R.; Takei, T.; Nguyen, N.-T. Surfactant-free, UV-curable core-shell microcapsules in a hydrophilic PDMS microfluidic device. *Aip Advances* **2020**, *10*.
27. Cacucciolo, V.; Shintake, J.; Kuwajima, Y.; Maeda, S.; Floreano, D.; Shea, H. Stretchable pumps for soft machines. *Nature* **2019**, *572*, 516-519.
28. Zhao, B.; Moore, J.S.; Beebe, D.J. Surface-directed liquid flow inside microchannels. *Science* **2001**, *291*, 1023-1026.
29. Pollack, M.G.; Fair, R.B.; Shenderov, A.D. Electrowetting-based actuation of liquid droplets for microfluidic applications. *Applied physics letters* **2000**, *77*, 1725-1726.
30. White, F.M.; Majdalani, J. *Viscous fluid flow*; McGraw-Hill New York: 2006; Volume 3.
31. Kovacs, G.T. *Micromachined transducers sourcebook*; WCB/McGraw-Hill New York: 1998; Volume 2.
32. Duprat, C.; Shore, H.A. *Fluid-structure interactions in low-Reynolds-number flows*; Royal Society of Chemistry: 2016.
33. Mao, W.; Caballero, A.; McKay, R.; Primiano, C.; Sun, W. Fully-coupled fluid-structure interaction simulation of the aortic and mitral valves in a realistic 3D left ventricle model. *PloS one* **2017**, *12*, e0184729.
34. Ma, T.; Sun, S.; Li, B.; Chu, J. Piezoelectric peristaltic micropump integrated on a microfluidic chip. *Sensors and Actuators A: Physical* **2019**, *292*, 90-96.
35. Gervais, T.; El-Ali, J.; Günther, A.; Jensen, K.F. Flow-induced deformation of shallow microfluidic channels. *Lab on a Chip* **2006**, *6*, 500-507.
36. Shidhore, T.C.; Christov, I.C. Static response of deformable microchannels: a comparative modelling study. *Journal of Physics: Condensed Matter* **2018**, *30*, 054002.
37. Hardy, B.S.; Uechi, K.; Zhen, J.; Kavehpour, H.P. The deformation of flexible PDMS microchannels under a pressure driven flow. *Lab on a Chip* **2009**, *9*, 935-938.
38. Anand, V.; Christov, I.C. Transient compressible flow in a compliant viscoelastic tube. *Physics of Fluids* **2020**, *32*.
39. Raj, M.K.; DasGupta, S.; Chakraborty, S. Hydrodynamics in deformable microchannels. *Microfluidics and Nanofluidics* **2017**, *21*, 1-12.
40. Christov, I.C.; Cognet, V.; Shidhore, T.C.; Stone, H.A. Flow rate-pressure drop relation for deformable shallow microfluidic channels. *Journal of Fluid Mechanics* **2018**, *841*, 267-286.
41. Ozsun, O.; Yakhot, V.; Ekinici, K.L. Non-invasive measurement of the pressure distribution in a deformable micro-channel. *Journal of Fluid Mechanics* **2013**, *734*, R1.
42. Cheung, P.; Toda-Peters, K.; Shen, A.Q. In situ pressure measurement within deformable rectangular polydimethylsiloxane microfluidic devices. *Biomicrofluidics* **2012**, *6*.
43. Chakraborty, D.; Prakash, J.R.; Friend, J.; Yeo, L. Fluid-structure interaction in deformable microchannels. *Physics of Fluids* **2012**, *24*.
44. Mehboudi, A.; Yeom, J. Experimental and theoretical investigation of a low-Reynolds-number flow through deformable shallow microchannels with ultra-low height-to-width aspect ratios. *Microfluidics and Nanofluidics* **2019**, *23*, 1-14.

45. Afrasiab, H.; Movahhedy, M.R.; Assempour, A. Fluid–structure interaction analysis in microfluidic devices: A dimensionless finite element approach. *International journal for numerical methods in fluids* **2012**, *68*, 1073-1086.
46. Bower, A.F. *Applied mechanics of solids*; CRC press: 2009.
47. Vannucci, P. *Continuum Mechanics-Solids*. **2017**.
48. Kim, T.K.; Kim, J.K.; Jeong, O.C. Measurement of nonlinear mechanical properties of PDMS elastomer. *Microelectronic Engineering* **2011**, *88*, 1982-1985.
49. Owen, B.; Kechagidis, K.; Bazaz, S.R.; Enjalbert, R.; Essman, E.; Mallorie, C.; Mirghaderi, F.; Schaaf, C.; Thota, K.; Vernekar, R. Lattice-Boltzmann Modelling for Inertial Particle Microfluidics Applications—A Tutorial Review. *bioRxiv* **2023**, 2023.2004.2010.536205.
50. Bruus, H. *Theoretical microfluidics*; Oxford university press: 2007; Volume 18.
51. Jiang, M.; Qian, S.; Liu, Z. Fully resolved simulation of single-particle dynamics in a microcavity. *Microfluidics and Nanofluidics* **2018**, *22*, 1-13.
52. Hübner, B.; Walhorn, E.; Dinkler, D. A monolithic approach to fluid–structure interaction using space–time finite elements. *Computer methods in applied mechanics and engineering* **2004**, *193*, 2087-2104.
53. Michler, C.; Hulshoff, S.; Van Brummelen, E.; De Borst, R. A monolithic approach to fluid–structure interaction. *Computers & fluids* **2004**, *33*, 839-848.
54. Ryzhakov, P.; Rossi, R.; Idelsohn, S.; Onate, E. A monolithic Lagrangian approach for fluid–structure interaction problems. *Computational mechanics* **2010**, *46*, 883-899.
55. Lin, Z.-h.; Li, X.-j.; Jin, Z.-j.; Qian, J.-y. Fluid-structure interaction analysis on membrane behavior of a microfluidic passive valve. *Membranes* **2020**, *10*, 300.
56. Przekwas, A.J.; Yang, H.; Athavale, M.M. Computational design of membrane pumps with active/passive valves for microfluidic MEMS. In *Proceedings of the Design, Test, and Microfabrication of MEMS and MOEMS*, 1999; pp. 266-277.
57. Jain, S.; Unni, H.N. Numerical modeling and experimental validation of passive microfluidic mixer designs for biological applications. *AIP Advances* **2020**, *10*.
58. Wen, C.Y.; Liang, K.P.; Chen, H.; Fu, L.M. Numerical analysis of a rapid magnetic microfluidic mixer. *Electrophoresis* **2011**, *32*, 3268-3276.
59. Hashim, U.; Diyana, P.A.; Adam, T. Numerical simulation of microfluidic devices. In *Proceedings of the 2012 10th IEEE International Conference on Semiconductor Electronics (ICSE)*, 2012; pp. 26-29.
60. Shahbazi, F.; Jabbari, M.; Esfahani, M.N.; Keshmiri, A. Numerical framework for simulating bio-species transport in microfluidic channels with application to antibody biosensors. *MethodsX* **2020**, *7*, 101132.
61. Mautner, T.S. Application of synthetic jets to low-Reynolds-number biosensor microfluidic flows for enhanced mixing: a numerical study using the lattice Boltzmann method. In *Proceedings of the Biomedical Applications of Micro-and Nanoengineering*, 2002; pp. 136-149.
62. Li, G.; Ye, T.; Wang, S.; Li, X.; UI Haq, R. Numerical design of a highly efficient microfluidic chip for blood plasma separation. *Physics of Fluids* **2020**, *32*.
63. Hung, P.J.; Lee, P.J.; Sabounchi, P.; Aghdam, N.; Lin, R.; Lee, L.P. A novel high aspect ratio microfluidic design to provide a stable and uniform microenvironment for cell growth in a high throughput mammalian cell culture array. *Lab on a Chip* **2005**, *5*, 44-48.
64. Erickson, D.; Li, D. Influence of surface heterogeneity on electrokinetically driven microfluidic mixing. *Langmuir* **2002**, *18*, 1883-1892.
65. Bianchi, F.; Ferrigno, R.; Girault, H. Finite element simulation of an electroosmotic-driven flow division at a T-junction of microscale dimensions. *Analytical Chemistry* **2000**, *72*, 1987-1993.
66. He, T.; Zhang, H.; Zhang, K. A smoothed finite element approach for computational fluid dynamics: applications to incompressible flows and fluid–structure interaction. *Computational Mechanics* **2018**, *62*, 1037-1057.
67. Orabona, E.; Rea, I.; Rendina, I.; Stefano, L.D. Numerical Optimization of a Microfluidic Assisted Microarray for the Detection of Biochemical Interactions. *Sensors* **2011**, *11*, 9658-9666.
68. Brebbia, C.A.; Telles, J.C.F.; Wrobel, L.C. *Boundary element techniques: theory and applications in engineering*; Springer Science & Business Media: 2012.
69. Kundu, P.K.; Cohen, I.M.; Dowling, D.R. *Fluid mechanics*; Academic press: 2015.
70. Martinez, A.W.; Phillips, S.T.; Wiley, B.J.; Gupta, M.; Whitesides, G.M. FLASH: a rapid method for prototyping paper-based microfluidic devices. *Lab on a Chip* **2008**, *8*, 2146-2150.

71. Li, X.; Tian, J.; Nguyen, T.; Shen, W. based microfluidic devices by plasma treatment. *Analytical chemistry* **2008**, *80*, 9131-9134.
72. Everstine, G.C.; Henderson, F.M. Coupled finite element/boundary element approach for fluid–structure interaction. *The Journal of the Acoustical Society of America* **1990**, *87*, 1938-1947.
73. Haile, J.M. *Molecular dynamics simulation: elementary methods*; John Wiley & Sons, Inc.: 1992.
74. Leimkuhler, B.; Reich, S. *Simulating hamiltonian dynamics*; Cambridge university press: 2004.
75. Liu, F.; Hu, N.; Ning, H.; Liu, Y.; Li, Y.; Wu, L. Molecular dynamics simulation on interfacial mechanical properties of polymer nanocomposites with wrinkled graphene. *Computational Materials Science* **2015**, *108*, 160-167.
76. Xue, C.; Wang, J.; Zhao, Y.; Chen, D.; Yue, W.; Chen, J. Constriction channel based single-cell mechanical property characterization. *Micromachines* **2015**, *6*, 1794-1804.
77. Zhang, L.T.; Gay, M. Immersed finite element method for fluid-structure interactions. *Journal of Fluids and Structures* **2007**, *23*, 839-857.
78. Xu, Y.; Liu, Y.; Xu, X.; Huang, G. Lattice Boltzmann simulation on molten carbonate fuel cell performance. *Journal of the Electrochemical Society* **2006**, *153*, A607.
79. Chen, S.; Chen, H.; Martinez, D.; Matthaeus, W. Lattice Boltzmann model for simulation of magnetohydrodynamics. *Physical Review Letters* **1991**, *67*, 3776.
80. Varnik, F.; Raabe, D. Lattice Boltzmann simulation of non-ideal fluids. In Proceedings of the RWTH Aachen Winter Semester 2007/2008.
81. Boghosian, B.M.; Coveney, P.V.; Emerton, A.N. A lattice-gas model of microemulsions. *Proceedings of the Royal Society of London. Series A: Mathematical, Physical and Engineering Sciences* **1996**, *452*, 1221-1250.
82. Hickey, O.A.; Holm, C.; Smiatek, J. Lattice-Boltzmann simulations of the electrophoretic stretching of polyelectrolytes: The importance of hydrodynamic interactions. *The Journal of chemical physics* **2014**, *140*.
83. Hammack, A.; Chen, Y.-L.; Pearce, J.K. Role of dissolved salts in thermophoresis of DNA: lattice-Boltzmann-based simulations. *Physical Review E* **2011**, *83*, 031915.
84. Hall, J.; Clarke, N. The mechanics of cilium beating: quantifying the relationship between metachronal wavelength and fluid flow rate. *Journal of Fluid Mechanics* **2020**, *891*, A20.
85. Lallemand, P.; Luo, L.-S. Lattice Boltzmann equation with Overset method for moving objects in two-dimensional flows. *Journal of Computational Physics* **2020**, *407*, 109223.
86. Dugast, F.; Favennec, Y.; Josset, C. Reactive fluid flow topology optimization with the multi-relaxation time lattice Boltzmann method and a level-set function. *Journal of Computational Physics* **2020**, *409*, 109252.
87. Tian, F.-B.; Luo, H.; Zhu, L.; Liao, J.C.; Lu, X.-Y. An efficient immersed boundary-lattice Boltzmann method for the hydrodynamic interaction of elastic filaments. *Journal of computational physics* **2011**, *230*, 7266-7283.
88. Feng, Z.-G.; Michaelides, E.E. The immersed boundary-lattice Boltzmann method for solving fluid–particles interaction problems. *Journal of computational physics* **2004**, *195*, 602-628.
89. Melchionna, S. A Model for Red Blood Cells in Simulations of Large-scale Blood Flows. *Macromolecular theory and simulations* **2011**, *20*, 548-561.
90. Wolf-Gladrow, D.A. *Lattice-gas cellular automata and lattice Boltzmann models: an introduction*; Springer: 2004.
91. Zhang, J. Lattice Boltzmann method for microfluidics: models and applications. *Microfluidics and Nanofluidics* **2011**, *10*, 1-28.
92. Bhatnagar, P.L.; Gross, E.P.; Krook, M. A model for collision processes in gases. I. Small amplitude processes in charged and neutral one-component systems. *Physical review* **1954**, *94*, 511.
93. Qian, Y.-H.; d'Humières, D.; Lallemand, P. Lattice BGK models for Navier-Stokes equation. *Europhysics letters* **1992**, *17*, 479.
94. Buick, J.M. Lattice Boltzmann methods in interfacial wave modelling. University of Edinburgh Edinburgh, 1997.
95. Yamaguchi, Y.; Honda, T.; Briones, M.P.; Yamashita, K.; Miyazaki, M.; Nakamura, H.; Maeda, H. Influence of Gravity on Two-Layer Laminar Flow in a Microchannel. *Chemical Engineering & Technology: Industrial Chemistry-Plant Equipment-Process Engineering-Biotechnology* **2007**, *30*, 379-382.
96. Li, D. *Electrokinetics in microfluidics*; Elsevier: 2004.
97. Qian, S.; Bau, H.H. Magneto-hydrodynamics based microfluidics. *Mechanics research communications* **2009**, *36*, 10-21.

98. Zhang, J.; Liu, Y.; Zhang, J.; Yang, J. Study of force-dependent and time-dependent transition of secondary flow in a rotating straight channel by the lattice Boltzmann method. *Physica A: Statistical Mechanics and its Applications* **2009**, *388*, 288-294.
99. Kang, Y.; Li, D. Electrokinetic motion of particles and cells in microchannels. *Microfluidics and nanofluidics* **2009**, *6*, 431-460.
100. He, X.; Zou, Q.; Luo, L.-S.; Dembo, M. Analytic solutions of simple flows and analysis of nonslip boundary conditions for the lattice Boltzmann BGK model. *Journal of Statistical Physics* **1997**, *87*, 115-136.
101. Abe, T. Derivation of the lattice Boltzmann method by means of the discrete ordinate method for the Boltzmann equation. *Journal of Computational Physics* **1997**, *131*.
102. Guo, Z.; Zheng, C.; Shi, B. Discrete lattice effects on the forcing term in the lattice Boltzmann method. *Physical review E* **2002**, *65*, 046308.
103. Shan, X.; Chen, H. Lattice Boltzmann model for simulating flows with multiple phases and components. *Physical review E* **1993**, *47*, 1815.
104. He, X.; Chen, S.; Doolen, G.D. A novel thermal model for the lattice Boltzmann method in incompressible limit. *Journal of computational physics* **1998**, *146*, 282-300.
105. Wang, J.; Wang, M.; Li, Z. Lattice Poisson-Boltzmann simulations of electro-osmotic flows in microchannels. *Journal of colloid and interface science* **2006**, *296*, 729-736.
106. Ladd, A.J.; Verberg, R. Lattice-Boltzmann simulations of particle-fluid suspensions. *Journal of statistical physics* **2001**, *104*, 1191-1251.
107. Guo, Z.; Zheng, C.; Shi, B. An extrapolation method for boundary conditions in lattice Boltzmann method. *Physics of fluids* **2002**, *14*, 2007-2010.
108. Le, G.; Zhang, J. Boundary slip from the immersed boundary lattice Boltzmann models. *Physical Review E* **2009**, *79*, 026701.
109. Zhang, J.; Kwok, D.Y. Pressure boundary condition of the lattice Boltzmann method for fully developed periodic flows. *Physical review E* **2006**, *73*, 047702.
110. Ladd, A.J. Numerical simulations of particulate suspensions via a discretized Boltzmann equation. Part 1. Theoretical foundation. *Journal of fluid mechanics* **1994**, *271*, 285-309.
111. Succi, S. *The lattice Boltzmann equation: for fluid dynamics and beyond*; Oxford university press: 2001.
112. Peskin, C.S. Numerical analysis of blood flow in the heart. *Journal of computational physics* **1977**, *25*, 220-252.
113. Bouzidi, M.h.; d'Humières, D.; Lallemand, P.; Luo, L.-S. Lattice Boltzmann equation on a two-dimensional rectangular grid. *Journal of Computational Physics* **2001**, *172*, 704-717.
114. Meng, X.; Wang, L.; Zhao, W.; Yang, X. Simulating flow in porous media using the lattice Boltzmann method: Intercomparison of single-node boundary schemes from benchmarking to application. *Advances in Water Resources* **2020**, *141*, 103583.
115. Filippova, O.; Hänel, D. Grid refinement for lattice-BGK models. *Journal of Computational physics* **1998**, *147*, 219-228.
116. Peng, C.; Teng, Y.; Hwang, B.; Guo, Z.; Wang, L.-P. Implementation issues and benchmarking of lattice Boltzmann method for moving rigid particle simulations in a viscous flow. *Computers & Mathematics with Applications* **2016**, *72*, 349-374.
117. Krüger, T.; Varnik, F.; Raabe, D. Efficient and accurate simulations of deformable particles immersed in a fluid using a combined immersed boundary lattice Boltzmann finite element method. *Computers & Mathematics with Applications* **2011**, *61*, 3485-3505.
118. Zhang, Y.; Pan, G.; Zhang, Y.; Haeri, S. A relaxed multi-direct-forcing immersed boundary-cascaded lattice Boltzmann method accelerated on GPU. *Computer Physics Communications* **2020**, *248*, 106980.
119. Inamuro, T. Lattice Boltzmann methods for moving boundary flows. *Fluid Dynamics Research* **2012**, *44*, 024001.
120. Wu, J.; Shu, C. Implicit velocity correction-based immersed boundary-lattice Boltzmann method and its applications. *Journal of Computational Physics* **2009**, *228*, 1963-1979.
121. Zhang, J.; Johnson, P.C.; Popel, A.S. Red blood cell aggregation and dissociation in shear flows simulated by lattice Boltzmann method. *Journal of biomechanics* **2008**, *41*, 47-55.
122. Sui, Y.; Low, H.; Chew, Y.; Roy, P. Tank-treading, swinging, and tumbling of liquid-filled elastic capsules in shear flow. *Physical Review E* **2008**, *77*, 016310.
123. Niu, X.; Shu, C.; Chew, Y.; Peng, Y. A momentum exchange-based immersed boundary-lattice Boltzmann method for simulating incompressible viscous flows. *Physics Letters A* **2006**, *354*, 173-182.

124. Dupuis, A.; Chatelain, P.; Koumoutsakos, P. An immersed boundary–lattice-Boltzmann method for the simulation of the flow past an impulsively started cylinder. *Journal of Computational Physics* **2008**, *227*, 4486-4498.
125. Schaaf, C.; Stark, H. Inertial migration and axial control of deformable capsules. *Soft matter* **2017**, *13*, 3544-3555.
126. Lashgari, I.; Ardekani, M.N.; Banerjee, I.; Russom, A.; Brandt, L. Inertial migration of spherical and oblate particles in straight ducts. *Journal of fluid mechanics* **2017**, *819*, 540-561.
127. Au, A.K.; Lai, H.; Utela, B.R.; Folch, A. Microvalves and micropumps for BioMEMS. *Micromachines* **2011**, *2*, 179-220.
128. Oh, K.W.; Ahn, C.H. A review of microvalves. *Journal of micromechanics and microengineering* **2006**, *16*, R13.
129. Unger, M.A.; Chou, H.-P.; Thorsen, T.; Scherer, A.; Quake, S.R. Monolithic microfabricated valves and pumps by multilayer soft lithography. *science* **2000**, *288*, 113-116.
130. Zheng, Y.; Dai, W.; Wu, H. A screw-actuated pneumatic valve for portable, disposable microfluidics. *Lab on a Chip* **2009**, *9*, 469-472.
131. Anjewierden, D.; Liddiard, G.A.; Gale, B.K. An electrostatic microvalve for pneumatic control of microfluidic systems. *Journal of Micromechanics and Microengineering* **2012**, *22*, 025019.
132. Bazargan, V.; Stoeber, B. Flow control using a thermally actuated microfluidic relay valve. *Journal of microelectromechanical systems* **2010**, *19*, 1079-1087.
133. Lv, J.; Jiang, Y.; Zhang, D.; Zhao, Y.; Sun, X. Characterization on the fatigue performance of a piezoelectric microvalve with a microfabricated silicon valve seat. *Journal of Micromechanics and Microengineering* **2013**, *24*, 015013.
134. Fordyce, P.; Diaz-Botia, C.; DeRisi, J.; Gomez-Sjoberg, R. Systematic characterization of feature dimensions and closing pressures for microfluidic valves produced via photoresist reflow. *Lab on a Chip* **2012**, *12*, 4287-4295.
135. Chang, H.-J.; Ye, W.; Kartalov, E.P. Quantitative modeling of the behaviour of microfluidic autoregulatory devices. *Lab on a Chip* **2012**, *12*, 1890-1896.
136. Zhang, X.; Zhu, Z.; Ni, Z.; Xiang, N.; Yi, H. Inexpensive, rapid fabrication of polymer-film microfluidic autoregulatory valve for disposable microfluidics. *Biomedical microdevices* **2017**, *19*, 1-9.
137. Zhang, X.; Zhang, Z. Microfluidic passive flow regulatory device with an integrated check valve for enhanced flow control. *Micromachines* **2019**, *10*, 653.
138. Nguyen, N.-T.; Truong, T.-Q.; Wong, K.-K.; Ho, S.-S.; Low, C.L.-N. Micro check valves for integration into polymeric microfluidic devices. *Journal of Micromechanics and Microengineering* **2003**, *14*, 69.
139. Kartalov, E.P.; Walker, C.; Taylor, C.R.; Anderson, W.F.; Scherer, A. Microfluidic vias enable nested bioarrays and autoregulatory devices in Newtonian fluids. *Proceedings of the National Academy of Sciences* **2006**, *103*, 12280-12284.
140. Yang, B.; Lin, Q. A planar compliance-based self-adaptive microfluidic variable resistor. *Journal of microelectromechanical systems* **2007**, *16*, 411-419.
141. Doh, I.; Cho, Y.-H. Passive flow-rate regulators using pressure-dependent autonomous deflection of parallel membrane valves. *Lab on a Chip* **2009**, *9*, 2070-2075.
142. Zhang, X.; Wang, X.; Chen, K.; Cheng, J.; Xiang, N.; Ni, Z. Passive flow regulator for precise high-throughput flow rate control in microfluidic environments. *RSC advances* **2016**, *6*, 31639-31646.
143. Chang, H.-T.; Wen, C.-Y.; Lee, C.-Y. Design, analysis and optimization of an electromagnetic actuator for a micro impedance pump. *Journal of Micromechanics and Microengineering* **2009**, *19*, 085026.
144. Kanakaris, G.; Fatsis-Kavalopoulos, N.; Alexopoulos, L. Laser activated single-use micropumps. *Sensors and Actuators B: Chemical* **2015**, *220*, 549-556.
145. Turkyilmazoglu, M. Mixed convection flow of magnetohydrodynamic micropolar fluid due to a porous heated/cooled deformable plate: exact solutions. *International Journal of Heat and Mass Transfer* **2017**, *106*, 127-134.
146. Lin, S.-C.; Lu, J.-C.; Sung, Y.-L.; Lin, C.-T.; Tung, Y.-C. A low sample volume particle separation device with electrokinetic pumping based on circular travelling-wave electroosmosis. *Lab on a Chip* **2013**, *13*, 3082-3089.
147. Shabani, R.; Cho, H.J. A micropump controlled by EWOD: wetting line energy and velocity effects. *Lab on a Chip* **2011**, *11*, 3401-3403.

148. Wang, X.Y.; Ma, Y.T.; Yan, G.Y.; Huang, D.; Feng, Z.H. High flow-rate piezoelectric micropump with two fixed ends polydimethylsiloxane valves and compressible spaces. *Sensors and Actuators A: Physical* **2014**, *218*, 94-104.
149. Ni, J.; Wang, B.; Chang, S.; Lin, Q. An integrated planar magnetic micropump. *Microelectronic engineering* **2014**, *117*, 35-40.
150. Lee, I.; Hong, P.; Cho, C.; Lee, B.; Chun, K.; Kim, B. Four-electrode micropump with peristaltic motion. *Sensors and Actuators A: Physical* **2016**, *245*, 19-25.
151. Hamid, N.A.; Majlis, B.Y.; Yunas, J.; Syafeeza, A.; Wong, Y.C.; Ibrahim, M. A stack bonded thermo-pneumatic micro-pump utilizing polyimide based actuator membrane for biomedical applications. *Microsystem Technologies* **2017**, *23*, 4037-4043.
152. Herzenberg, L.A.; Sweet, R.G.; Herzenberg, L.A. Fluorescence-activated cell sorting. *Scientific American* **1976**, *234*, 108-118.
153. Shields Iv, C.W.; Reyes, C.D.; López, G.P. Microfluidic cell sorting: a review of the advances in the separation of cells from debulking to rare cell isolation. *Lab on a Chip* **2015**, *15*, 1230-1249.
154. Sun, C.; Munn, L.L. Lattice-Boltzmann simulation of blood flow in digitized vessel networks. *Computers & Mathematics with Applications* **2008**, *55*, 1594-1600.
155. Mao, W.; Alexeev, A. Hydrodynamic sorting of microparticles by size in ridged microchannels. *Physics of Fluids* **2011**, *23*.
156. Hosseini, S.M.; Feng, J.J. How malaria parasites reduce the deformability of infected red blood cells. *Biophysical journal* **2012**, *103*, 1-10.
157. Khodaei, F.; Movahed, S.; Fatouraei, N.; Daneshmand, F. Numerical simulation of separation of circulating tumor cells from blood stream in deterministic lateral displacement (DLD) microfluidic channel. *Journal of Mechanics* **2016**, *32*, 463-471.
158. Nguyen, N.-T.; Wu, Z. TOPICAL REVIEW: Micromixers—a review. *Journal of Micromechanics and Microengineering* **2005**, *15*, R1-R16.
159. Ahmed, D.; Mao, X.; Juluri, B.K.; Huang, T.J. A fast microfluidic mixer based on acoustically driven sidewall-trapped microbubbles. *Microfluidics and nanofluidics* **2009**, *7*, 727-731.
160. Luong, T.-D.; Phan, V.-N.; Nguyen, N.-T. High-throughput micromixers based on acoustic streaming induced by surface acoustic wave. *Microfluidics and nanofluidics* **2011**, *10*, 619-625.
161. Campisi, M.; Accoto, D.; Damiani, F.; Dario, P. A soft-lithographed chaotic electrokinetic micromixer for efficient chemical reactions in lab-on-chips. *Journal of Micro-Nano Mechatronics* **2009**, *5*, 69-76.
162. Lim, C.Y.; Lam, Y.C.; Yang, C. Mixing enhancement in microfluidic channel with a constriction under periodic electro-osmotic flow. *Biomicrofluidics* **2010**, *4*.
163. Xu, B.; Wong, T.N.; Nguyen, N.-T.; Che, Z.; Chai, J.C.K. Thermal mixing of two miscible fluids in a T-shaped microchannel. *Biomicrofluidics* **2010**, *4*.
164. Wang, Y.; Zhe, J.; Chung, B.T.; Dutta, P. A rapid magnetic particle driven micromixer. *Microfluidics and Nanofluidics* **2008**, *4*, 375-389.
165. Lam, Y.; Gan, H.; Nguyen, N.-T.; Lie, H. Micromixer based on viscoelastic flow instability at low Reynolds number. *Biomicrofluidics* **2009**, *3*.
166. Buchegger, W.; Wagner, C.; Lendl, B.; Kraft, M.; Vellekoop, M.J. A highly uniform lamination micromixer with wedge shaped inlet channels for time resolved infrared spectroscopy. *Microfluidics and Nanofluidics* **2011**, *10*, 889-897.
167. Tofteberg, T.; Skolimowski, M.; Andreassen, E.; Geschke, O. A novel passive micromixer: lamination in a planar channel system. *Microfluidics and Nanofluidics* **2010**, *8*, 209-215.
168. Kang, T.; Singh, M.; Anderson, P.; Meijer, H. A Chaotic Serpentine Mixer Efficient in the Creeping Flow Regime From Design Concept to Optimization, *Microfluid.* **2009**.
169. Neerincx, P.E.; Denteneer, R.P.; Peelen, S.; Meijer, H.E. Compact mixing using multiple splitting, stretching, and recombining flows. *Macromolecular Materials and Engineering* **2011**, *296*, 349-361.
170. Lin, C.-H.; Tsai, C.-H.; Fu, L.-M. A rapid three-dimensional vortex micromixer utilizing self-rotation effects under low Reynolds number conditions. *Journal of Micromechanics and Microengineering* **2005**, *15*, 935.
171. Tsai, R.-T.; Wu, C.-Y. An efficient micromixer based on multidirectional vortices due to baffles and channel curvature. *Biomicrofluidics* **2011**, *5*.

172. Lin, C.-Y.; Chen, C.-Y.; Hu, Y.-T.; Chen, C.-Y. Fluid dynamics analysis of magnetically actuated ciliated nano/micro structures for flow mixing and propulsion applications. In Proceedings of the The 8th Annual IEEE International Conference on Nano/Micro Engineered and Molecular Systems, 2013; pp. 590-593.
173. Talebjedi, B.; Ghazi, M.; Tasnim, N.; Janfaza, S.; Hoorfar, M. Performance optimization of a novel passive T-shaped micromixer with deformable baffles. *Chemical Engineering and Processing-Process Intensification* **2021**, *163*, 108369.
174. Laha, S.; Fourtakas, G.; Das, P.K.; Keshmiri, A. Fluid–structure interaction modeling of bi-leaflet mechanical heart valves using smoothed particle hydrodynamics. *Physics of Fluids* **2023**, *35*.
175. Sodhani, D.; Reese, S.; Aksenov, A.; Soğancı, S.; Jockenhövel, S.; Mela, P.; Stapleton, S.E. Fluid-structure interaction simulation of artificial textile reinforced aortic heart valve: Validation with an in-vitro test. *Journal of biomechanics* **2018**, *78*, 52-69.
176. Lee, J.H.; Rygg, A.D.; Kolahdouz, E.M.; Rossi, S.; Retta, S.M.; Duraiswamy, N.; Scotten, L.N.; Craven, B.A.; Griffith, B.E. Fluid–structure interaction models of bioprosthetic heart valve dynamics in an experimental pulse duplicator. *Annals of biomedical engineering* **2020**, *48*, 1475-1490.
177. Gilmanov, A.; Stolarski, H.; Sotiropoulos, F. Non-linear rotation-free shell finite-element models for aortic heart valves. *Journal of biomechanics* **2017**, *50*, 56-62.
178. Sigüenza, J.; Pott, D.; Mendez, S.; Sonntag, S.J.; Kaufmann, T.A.; Steinseifer, U.; Nicoud, F. Fluid-structure interaction of a pulsatile flow with an aortic valve model: a combined experimental and numerical study. *International journal for numerical methods in biomedical engineering* **2018**, *34*, e2945.
179. Pabi, S.; Khan, M.; Jain, S.K.; Sen, A.K.; Raj, A. Effect of stenotic shapes and arterial wall elasticity on the hemodynamics. *Physics of Fluids* **2023**, *35*.
180. Campobasso, R.; Condemi, F.; Viallon, M.; Croisille, P.; Campisi, S.; Avril, S. Evaluation of peak wall stress in an ascending thoracic aortic aneurysm using FSI simulations: effects of aortic stiffness and peripheral resistance. *Cardiovascular engineering and technology* **2018**, *9*, 707-722.
181. Guerciotti, B.; Vergara, C.; Ippolito, S.; Quarteroni, A.; Antona, C.; Scrofani, R. Computational study of the risk of restenosis in coronary bypasses. *Biomechanics and modeling in mechanobiology* **2017**, *16*, 313-332.
182. van Bakel, T.M.; Arthurs, C.J.; Nauta, F.J.; Eagle, K.A.; van Herwaarden, J.A.; Moll, F.L.; Trimarchi, S.; Patel, H.J.; Figueroa, C.A. Cardiac remodelling following thoracic endovascular aortic repair for descending aortic aneurysms. *European Journal of Cardio-Thoracic Surgery* **2019**, *55*, 1061-1070.
183. Jayendiran, R.; Nour, B.; Ruimi, A. Computational fluid–structure interaction analysis of blood flow on patient-specific reconstructed aortic anatomy and aneurysm treatment with Dacron graft. *Journal of Fluids and Structures* **2018**, *81*, 693-711.
184. Valente, R.; Mourato, A.; Brito, M.; Xavier, J.; Tomás, A.; Avril, S. Fluid–structure interaction modeling of ascending thoracic aortic aneurysms in simvascular. *Biomechanics* **2022**, *2*, 189-204.

Disclaimer/Publisher's Note: The statements, opinions and data contained in all publications are solely those of the individual author(s) and contributor(s) and not of MDPI and/or the editor(s). MDPI and/or the editor(s) disclaim responsibility for any injury to people or property resulting from any ideas, methods, instructions or products referred to in the content.